PFC/JA-91-30

Alpha Particle Losses From Toroidicity Induced Alfvén Eigenmodes, Part II: Monte Carlo Simulations and Anomalous Alpha Loss Processes

D. J. Sigmar and C. T. Hsu
R. White* and C. Z. Cheng*

April 1992

Plasma Fusion Center
Massachusetts Institute of Technology
Cambridge, MA 02139 USA

*Princeton University, Plasma Physics Laboratory, Princeton, NJ 08543 USA

This work was supported by the US Department of Energy under contract DE-FG02-91ER-54109. Reproduction, translation, publication, use, and disposal, in whole or in part, by or for the US Government is permitted.

Submitted for publication in **Physics of Fluids B**

ALPHA PARTICLE LOSSES FROM TOROIDICITY INDUCED ALFVÉN EIGENMODES

Part II: Monte Carlo Simulations and Anomalous Alpha Loss Processes

D. J. SIGMAR and C. T. HSU

Massachusetts Institute of Technology, Plasma Fusion Center, 167 Albany Street, NW16-250, Cambridge, MA 02139 USA, Tel: (617) 253-0513

R. WHITE and C. Z. CHENG

Princeton University, Plasma Physics Laboratory, Princeton, NJ 08543 USA

Abstract

Fusion born α particles moving parallel to the magnetic field can resonate with toroidal Alfvén eigenmodes (TAE) leading to anomalous α orbit diffusion across the α loss boundaries in a tokamak. This is analyzed using the Hamiltonian guiding center code ORBIT in conjunction with the kinetic magnetohydrodynamics (MHD) eigenmode solving code Nova-K. Resonant single α orbits are studied below and above the threshold for orbit stochasticity and Monte Carlo randomized ensembles of alphas subjected to a finite amplitude time dependent TAE are followed with respect to their radial losses using realistic MHD equilibria and numerically computed toroidal Alfvén eigenfunctions for one toroidal eigenmode $n = 1$ and the full Fourier spectrum of poloidal harmonics m involved in the "gap mode." The α loss mechanisms are resonant drift motion across the loss boundaries of alphas born near these boundaries and stochastic diffusion to the boundaries in constants of the motion (phase) space. After a first transient of resonant drift losses scaling as $\tilde{B}_r/B_0$, the number of alphas lost via diffusion scales as $(\tilde{B}_r/B_0)^2$. For TAE amplitudes $\tilde{B}_r/B_0 \geq 10^{-3}$ α orbit stochasticity sets in and, depending on the radial width of the fast α density $n_\alpha(r)$, a substantial fraction of alphas can be lost in one slowing down time. For $\tilde{B}_r/B_0 < 10^{-4}$ the losses become insignificant.

Submitted to **Physics of Fluids B**, September 1991

I. INTRODUCTION

Until recently, the fusion born energetic alphas were assumed to be classically confined during their collisional slowing down on the bulk electrons and ions in the tokamak. This notion was supported by the apparently classical equilibration of neutral beam injected ions with beam energies $E_b \leq 150$ keV. However, the 3.5 MeV α velocity is typically 1.5-2 times faster than the Alfvén speed v_A of the plasma which gives rise to Cherenkov excitation of Alfvén waves and anomalous α losses.

The ensuing theoretical possibility of resonant interaction between fusion born alphas travelling parallel to the magnetic field and shear Alfvén waves $\omega_A = k_{\|} v_A$ was recognized by Mikhailovski[1] and Rosenbluth[2] over 15 years ago and solved numerically in Ref. 3. When the free energy of the centrally peaked α particle density is included one finds a linear instability if $\omega_{*\alpha} > \omega_A$. (Here $\omega_{*\alpha}$ is the α diamagnetic frequency.) Nonlinearly, an anomalous fast α diffusion coefficient D_α^{an} can result which becomes important when $\tau_\alpha^{-1} \equiv \frac{4D_\alpha^{an}}{a^2} > \tau_{SD}^{-1}$ where a is the minor radius of the plasma and τ_{SD} is the α particle slowing down time. Two recent tokamak experiments[4,5] with parallel neutral beam injection have demonstrated the essential features of super-Alfvénic ion losses due to excited Toroidal Alfvén Eigenmodes (TAE)[6,7,8,9]. The subject of the present work is the calculation of τ_α due to the TAE spectrum[10] in burning tokamak plasmas such as the Compact Ignition Tokamak (CIT)[11] and the International Thermonuclear Experimental Reactor (ITER).[12]

In Section II, the toroidal Alfvén eigenmode structure is introduced, analytically and numerically. The α kinetic resonance with the TAE produces an α energy exchange with the mode which, because of the finite α orbit width, is treated numerically as a two dimensional (2-D) problem. Since $\omega_A < \Omega_\alpha$ (the α gyrofrequency) a guiding center description is adopted. Its Hamiltonian formalism is described in Section III. The α Alfvén wave resonance gives rise to an anomalous radial guiding center drift. Above a critical amplitude $(\tilde{B}_r/B_0)_{crit}$, α orbit stochasticity sets in. Section IV is devoted to numerical studies of single α orbits in Subsection IV.1, a Monte Carlo simulation of relatively short duration (of 200 α transit times) in a circularized CIT equilibrium, in Subsection IV.2, and an extended

(up to 5000 $\tau_{transit}$) Monte Carlo simulation showing stochastic diffusion in constants of the motion space in a D-shaped CIT equilibrium in Subsection IV.3. The properties of the α orbit stochastic maps and their significance for transport across the α loss boundaries are developed in Section V. Section VI gives a summary and conclusions. Finally, numerical accuracy of the orbit integrator and the Monte Carlo simulation are briefly discussed in an Appendix.

II. LINEAR MODE THEORY

1. Linear TAE Spectrum

Lately the linear theory of the TAE has received a great deal of theoretical attention[13,14] and we refer to these papers. For present purposes it suffices to recall the linear mode structure for a given toroidal mode number n

$$\begin{aligned}\tilde{A}_{\|} &= \sum_m A_m(\psi)\cos[(-n\zeta + m\theta - \omega t)] \\ &\equiv \sum_m A_m(\psi)\cos\Phi_m \end{aligned} \tag{1}$$

where the poloidal mode numbers contain two principle m-numbers such that the flux surface where $k^2_{\|m} = k^2_{\|m+1}$ defines the "gap" location $q_{gap} = \frac{m+1/2}{n}$ (valid for circular plasma cross section. For D-shaped plasmas cf. Ref. 14. (Here $k_{\|} = (n - \frac{m}{q(\psi)})/R_0$ is the parallel wave vector and $q(\psi)$ the radial safety factor profile.) The radius r_{gap} where $q = q_{gap}$ is called gap radius. The real frequency of the TAE is $\omega_r = k_{\|}v_A = v_A/2R_0q_{gap}$. The ideal magnetohydrodynamics (MHD) shear Alfvén wave has $\tilde{B}_{\|} = 0$,

$$\tilde{E}_{\|} = -\nabla_{\|}\tilde{\phi} - \frac{1}{c}\frac{\partial \tilde{A}_{\|}}{\partial t} = 0$$

or

$$\tilde{\phi} = \frac{\omega}{ck_{\|}}\tilde{A}_{\|} \tag{2}$$

We write

$$\tilde{\phi} = \sum_m \phi_m(r)\cos\Phi_m \tag{3a}$$

and using $\tilde{B} = \nabla \times \tilde{A}_{\|}\mathbf{b}$ there results, for a given poloidal harmonic

$$
\begin{aligned}
B_r^m &= -\frac{ck_{\|}}{\omega}\frac{m}{r}\phi_m \sin\Phi_m \\
B_\theta^m &= -\frac{ck_{\|}}{\omega}\frac{\partial\phi_m}{\partial r}\cos\Phi_m \\
E_r^m &= -\frac{\partial\phi_m}{\partial r}\cos\Phi_m \\
\tilde{E}_\theta &= \frac{m}{r}\phi_m \sin\Phi_m
\end{aligned}
\tag{3b}
$$

The flux surface radius r is related to the flux label ψ_p. (In our numerical work we use normalized toroidal flux $\psi_T = \left(\frac{r}{a}\right)^2/2$ for circular plasma cross section cases and poloidal flux $\psi_p = \int d\psi_T/q$ for noncircular equilibria.) We note from Eqs. (3b) that while $\tilde{E}_\theta$ peaks at $r = r_{gap}$, $\tilde{B}_r$ will peak elsewhere, depending on $\frac{1}{r}k_{\|}(r)$. We normalize $\tilde{A}_{\|}$ such that

$$\tilde{\alpha} \equiv \tilde{A}_{\|}/R_0 B \tag{4a}$$

where R_0 is the major radius and B_0 the equilibrium B-field and we will frequently refer to the peak amplitude of $\tilde{\alpha}$ as a measure of the strength of the TAE perturbation. Using $\tilde{\alpha}$, one can write

$$\tilde{\mathbf{B}} = \nabla \times \tilde{\alpha}\mathbf{B}R_0 \tag{4b}$$

Typically, $\frac{\tilde{B}_r}{B_0} \geq \tilde{\alpha}$.

2. Alpha Kinetic Resonance with TAE

The resonance condition for passing alphas

$$\omega - k_{\|}v_{\|\alpha} - \mathbf{k}_\perp \cdot \mathbf{v}_{D\alpha} = 0$$

can be readily satisfied for $\omega = k_{\|}v_A$ and $v_{\|\alpha} \gtrsim v_A$. Invoking poloidal sidebands resonance occurs also for $v_{\|\alpha} < v_A$.[14] The retention of the magnetic drift term is essential for the

wave-particle interaction since, with $\tilde{E}_{\|} = 0$,

$$\begin{aligned} \frac{dE_\alpha}{dt} &= e_\alpha \mathbf{v}_{gc\alpha} \cdot \tilde{\mathbf{E}} \propto \mathbf{v}_{D\alpha} \cdot \nabla \tilde{\phi} \\ &\propto v_{Dr} \frac{\partial \tilde{\phi}}{\partial r} + (v_{D\theta}/r) \frac{\partial \tilde{\phi}}{\partial \theta} \\ &\propto k_r v_{Dr} \tilde{\phi} + \frac{m}{r} v_{D\theta} \tilde{\phi} \end{aligned} \tag{5}$$

Equation (5) shows that the magnetic drift in the θ direction can dominate over the radial drift in the core region of the burning plasma thus making this a 2-D problem. This fact, combined with the large orbit width of the fast alphas has led us to adopt a numerical approach for the α guiding center TAE interaction study, very interesting analytic work[15,16] for varying ratio of mode width to α orbit width notwithstanding.

III. HAMILTONIAN GUIDING CENTER MOTION OF THE ALPHA PARTICLE MOTION IN THE WAVE FIELD

1. Hamiltonian Formulation

A Hamiltonian formalism[17,18,19] is useful for enhancing the numerical accuracy of the orbit integrator with respect to the constants of the motion as well as to avoid numerical stochasticity in the area preserving orbit maps to be shown further below.

Starting from Morozov and Solovév[17] and Littlejohn[18] (to produce a Hamiltonian form and satisfy Liouville's theorem) we have for the α drift motion

$$\vec{v}_D = \frac{v_{\|}/B}{1 + \rho_{\|} \vec{b} \cdot \nabla \times \vec{b}} (\vec{B} + \nabla \times \rho_{\|} \vec{B}); \quad \rho_{\|} \equiv \frac{v_{\|}}{\Omega}$$

which leads to the Hamiltonian

$$H_{GC} = \frac{1}{2} \rho_{\|}^2 B^2 + \mu B + e\phi$$

The shear Alfvén perturbation is introduced through[20]

$$\delta \vec{B} = \nabla \times \tilde{\alpha} \vec{B}, \quad \tilde{\alpha} = \sum \alpha_{mn}(\psi) \cos(m\theta - n\xi - \omega t)$$

Letting $\rho_c \equiv \rho_{||} + \tilde{\alpha}$ permits inclusion of the perturbation $\tilde{\alpha}$ in the Hamiltonian as

$$H = \frac{1}{2}(\rho_c - \tilde{\alpha})^2 B^2 + \mu B + e\phi$$

with four Hamiltonian variables

$$\xi, \theta, P_\xi \equiv g\rho_c - \psi_p, P_\theta \equiv I\rho_c + \psi_T$$

where $g = RB_\phi$, $I(\psi)$ is the toroidal current inside ψ and ψ_T is the toroidal flux. One has

$$\dot{P}_\xi = -\frac{\partial H}{\partial \xi} \qquad \dot{\xi} = \frac{\partial H}{\partial P_\xi}$$

$$\dot{P}_\theta = -\frac{\partial H}{\partial \theta} \qquad \dot{\theta} = \frac{\partial H}{\partial P_\theta}$$

Also, one finds expressions for the radial drift $\dot{\psi} = \dot{\psi}(\tilde{\alpha}, \dot{\tilde{\alpha}})$ and the parallel acceleration $\dot{\rho}_{||} = \dot{\rho}_{||}(\tilde{\alpha}, \dot{\tilde{\alpha}})$ describing both classical drift- and perturbed α-orbit motion. The radial α particle drift velocity is

$$\dot{\psi}_p = \frac{g(\rho_{||}^2 + \mu)}{D}\frac{\partial B}{\partial \theta} + A\alpha_{nm}\cos(n\xi - m\theta - \omega t)$$

where D and A are equilibrium quantities defined on pages 71 and 254 of Ref. 20 and $\xi(t), \theta(t)$ describe the toroidal and poloidal guiding center drift motion. The first term gives the "banana" width, the second term can become secular if $\omega \simeq \omega_d$, describing the resonant radial α drift which can take the α particle to the loss boundary of the finite tokamak geometry.

2. Resonant and Stochastic Alpha Motion

Indeed, the condition $\frac{dE_\alpha}{dt} \propto \mathbf{v}_d \cdot \nabla\tilde{\phi} = \text{const.}$ is essentially the condition $\omega = k_{||}v_{||} + \mathbf{k}_\perp \mathbf{v}_d$ along an orbit. When $\frac{dE_\alpha}{dt} \neq 0$, the α pitch angle $\lambda \equiv \mu B_0/E_\alpha$ will change while μ is conserved ($\omega_A \ll e_\alpha B/m_\alpha c$). A frequently observed event is the resonant conversion of a passing α near the passing/trapped boundary into a fat banana orbit. When the orbit width Δ_α is comparable to the radial mode width $\Delta_m \sim \epsilon r_{gap}$ of the

global (where $\epsilon = a/R_0$) the resonant drive can be maintained for several transit times. This condition is satisfied for energetic alphas near the trapped/passing boundary, for low mode numbers n, m. For high mode numbers the α guiding center traversing the more narrow mode width Δ_m suffers a shorter resonant kick.[16,21] For both conditions, α orbit stochasticity will be shown to occur at sufficiently large amplitude of $\tilde{B}_r/B_0$. This can lead to stochastic diffusion in α guiding center phase space. Typical α orbit widths are shown in Fig. 1.

Thus, one expects three mechanisms of α losses from the system. The first is resonant drift of an α born near a loss boundary, the second is the above mentioned resonant conversion of a barely passing α into a fat α-banana intersecting the wall and the third is sustained stochastic diffusion in $P_\varphi - E - \lambda$ space until the α is swept across an orbit loss boundary. These loss boundaries are shown in Fig. 2 and are the subject of Part I of the present work.[22] In the next section we will show α guiding center Monte Carlo simulations with two different loss boundary scenarios.

IV. ALPHA GUIDING CENTER SIMULATIONS

In this section we investigate numerically the resonant α losses due to the gap mode fluctuations. Given machine parameters, q-profile and mode numbers, a numerical solution for the radial eigenfunctions $\phi_m(\psi)$ of Eq. (3a) is produced with the Nova-K code.[13] Then, $\tilde{B}$ and $A_{||}$ follow from

$$\tilde{A}_{||} = \frac{k_{||}c}{w}\tilde{\phi}, \quad \tilde{B} = \nabla \times \tilde{A}_{||}\vec{b} = \nabla \times \tilde{\alpha}\vec{B}R_o$$

where B is the equilibrium field. Figures 3 and 4 show the toroidal Alfvén radial eigenfunctions vs. ψ_T and ψ_p, the toroidal and poloidal flux variables such that $\psi_{Tb} = 0.5$ and $\psi_{pb} = 0.147$ at the plasma boundary.

Next, the parameter $\tilde{\alpha}$ corresponding to a given amplitude $\frac{\tilde{B}}{B_o}$ is prescribed. Typically, we vary

$$\frac{\tilde{B}_r}{B_o} = 10^{-5}, 10^{-4}, 10^{-3} \ .$$

Up to 5120 particles are followed for up to 5000 transit times. v and ψ are chosen fixed or with a certain spread, and and $\frac{v_\parallel}{v}, \theta$ are distributed randomly. Two types of studies are carried out:

(i) single guiding center orbits, subject to the motion in the equilibrium field B_0 and the time dependent fluctuations $\tilde{B}, \tilde{\phi}$ (where we monitor α particle resonances and ensuing loss details;

(ii) ensemble of guiding centers, monitoring loss rate, $N_{\rm tot}$ (lost) and properties of lost (or "exiting") alphas.

The choice of perturbation amplitude is not arbitrary but guided by experimental values for low mode number MHD-like perturbations. For example, in the TEXT tokamak,[23] $\tilde{B}_r/B_o(f > 50 \text{ kHz}) \sim 10^{-5}$ has been observed near the edge; in the so-called β collapse of the Tokamak Fusion Test Reactor (TFTR),[24] $\tilde{B}_r/B_o \sim 10^{-4}$ is estimated; and for the fishbone oscillations in the Princeton Beta Experiment (PDX),[25] $\tilde{B}_r/B_o \gtrsim 10^{-3}$ was observed. Close to disruptions, Mirnov oscillations can exceed $\tilde{B}_\theta/B_o \sim 10^{-4}$. The TAE amplitude was not determined in the two experiments[4,5] but, judging from the observed fast ion losses, should approach the fishbone amplitudes (cf. also Ref. 26). An analytic stochastic onset calculation[21] gives $\tilde{B}_r/B_0 \simeq 10^{-3}$.

Exposing the α particles to only one toroidal mode number is expected to produce a conservative loss rate (cf. Ref. 21). Furthermore, mode coupling effects neglected here may indeed be unimportant for the saturation of the TAE (cf. Ref. 27).

1. Characteristic Single Particle Orbits

As a first simplified case, (presented previously, cf. Ref. 7a) first we assume a circularized CIT equilibrium specified in Appendix A. Starting in the untrapped pitch angle region, an α particle of energy $E_o = 3.5$ MeV near the center ($r_o/a = .1$) becomes resonant with the Alfvén wave and loses energy to the wave thereby undergoing a resonant radial outward excursion. Near the edge, the α particle is scattered by the fluctuation (Coulomb collisions are excluded throughout this work) into the trapped region which constitutes a prompt loss

orbit. Figures 5a,b,c show an important class of orbits for $B_r/B_0 = 5 \times 10^{-3}$ in a circular plasma cross section, where the TAE of Fig. 3 has been used. Figure 5a shows the fractional energy loss $\frac{\Delta E}{E_o}$ as a function of time, measured in units of $\tau_{transit} \equiv (v_o/2\pi R_o)^{-1}$. Figure 5b shows the evolution of the pitch angle variable $v_{||}/v$. Figure 5c shows the orbit in the $r - \theta$ plane terminating at the wall.

Figures 6 show a similar passing α orbit in a D-shaped cross section for CIT equilibrium B (see Appendix A) for the eigenfunctions of Fig. 4. Note in both cases that resonant interaction of the passing α launched near the passing/trapped boundary lasts for 2-3 transit periods at a time, reducing E_α. This finally increases the pitch angle variable $\lambda = \mu B_0/E$ enough to trap the α as can be seen clearly when $\frac{v_{||}}{v}$ goes through zero. The trapped α is on a loss orbit, i.e., it intersects the plasma boundary. This class of orbit losses has been identified to play an important role in TFTR fast ion experiments.[28] Likewise, as will be shown in the next section, this type of loss of barely passing alphas dominates the loss statistics in the guiding center Monte Carlo simulation. As a subdominant effect, we have observed a small percentage of initially **trapped** fat α- bananas precessing toroidally and exhibiting resonance with the TAE such that the banana center drifts radially outward until it is scraped off at the plasma boundary in the outer midplane.

2. Monte Carlo Simulation of Alpha Particle Ensemble in a Simple Circularized Plasma Case

For the circular cross section eigenfunction of Fig. 3, we consider in this first study an initial ensemble of 5120 particles localized at $r_o/a = .5$, with randomly distributed poloidal angle and pitch angle with energy 3 MeV $\leq$ 3.52 MeV. $B_r/B_o = 5 \times 10^{-4}$ is assumed and the α loss rate is monitored as a function of time. Figure 7a shows the final spread out radial distribution after 200 transit times (which ends the run). Figure 7b shows the energy distribution of those alphas which hit the wall due to their resonant energy exchange and ensuing outward drift. Figure 7c shows the loss rate $\nu_L \equiv \frac{\Delta N_{lost}}{N_{total}\Delta t}$ where Δt is coarsegrained (averaged) over $5\tau_{transit}$. The initially large prompt orbit losses have evanesced after $\approx 40\tau_{transit}$. In this simulation, we replace each lost α resonantly

drifting across the plasma boundary by another one at a **randomly chosen** phase space point. These alphas can be born near the plasma boundary and dominate the observed losses. Losses of alphas having stochastically diffused from "inner" regions of phase space would scale as $(\tilde{B}/B_0)^2$ do not have a chance to be observed in this case.

In a second run of this study for the same circularized equilibrium we assume a radially spread out birth distribution, namely

$$n_\alpha(r) = \begin{cases} n_\alpha(o)(1-(r/a)^4)^4, & r/a < 0.75 \\ 0, & r/a > 0.75 \end{cases}$$

(truncated to avoid trivial prompt losses near the plasma edge). This shape is derived from the assumed pressure profile $\beta \propto (1-(r/a)^4)^2)$. Taking $\frac{\tilde{B}_r}{B} = 5 \times 10^{-4}$ we find the loss rate $\nu_{loss} \simeq 10^2 s^{-1}$, i.e. $\tau_{loss} \simeq 10$ ms$\simeq \frac{1}{4}\tau_{SD}$. Noting that the fusion α particle production rate at $T = 10$ keV, $n_e = 5 \times 10^{14}$ cm^{-3} is about 60 s^{-1}, the TAE mode losses can overwhelm the fusion α production unless $\frac{\tilde{B}_r}{B_o} < 10^{-4}$ in this simulation.

Another series of runs was made involving an initial ensemble of 512 particles with a randomly distributed poloidal angle, pitch angle, and box-like radial density profile (cut off $r/a \leq 0.7$ to minimize prompt losses outside of this radius). The initial energy was randomly distributed within a given range as shown in Table 1. The results of those Monte Carlo simulations are summarized as follows (see also Table 1):

1. Roughly, $\nu_{loss} = (2 \times 10^6)\tilde{\alpha}$, i.e. proportional to $\tilde{B}_r/B_0$. This linear scaling can be understood from the formula for $\dot{\psi}_p$ given above.

2. For the energy group $E_o < 1.5$ MeV, the loss is insignificant. For $2.52 \leq E_o \leq 3.52$ (i.e. the initial particle kinetic energy is randomly distributed between 2.52 and 3.52 MeV) and $\tilde{\alpha} = 10^{-4}$ (i.e. $\frac{\tilde{B}_r}{B} = 5 \times 10^{-4}$), we have $\tau_{loss} = 4$ ms $\simeq \frac{1}{10}\tau_{SD}$.

Note that as shown in Fig. 7, all of the above runs were terminated after only 200 α transit times. Longer runs (to be discussed next) are necessary to demonstrate the final steady state α loss level. They are described in the next section.

3. Extended Monte Carlo Simulation in D-Shaped Plasma

The CIT equilibrium parameters for this second study are given in Appendix A (equilibrium B) and the corresponding radial structure of the TAE poloidal harmonics is shown in Fig. 4. Besides these MHD modifications from the run in Section IV.2, a number of important changes have been made to address open questions and obtain a deeper understanding. First and foremost, using the theory of Ref. 22 all relevant loss boundaries in phase space have been worked out for the equilibrium magnetic field geometry and alphas crossing the loss boundaries are **not** replaced, in order to clearly bring out the stochastic phase space diffusion driven losses. Second, the run time is extended to 1000-5000 $\tau_{transit}$. Third, the relative orbit width in the D-shaped cross section shown in Fig. 1 is smaller than that of the circular equilibrium A, but more importantly, by following the alphas in constants of the motion (COM) space rather than in configuration space, appropriate diffusion coefficients can be formulated[22] and measured in the simulation. Fourth, we have constructed the Poincaré plots of the α guiding center orbits for each assumed value of $\tilde{B}_r/B_0$ and have determined the stochastic threshold. Consequently, the location of th KAM surfaces in $P_\varphi - \lambda$ space reveals the split between resonant drift losses $\propto \tilde{B}_r/B_0$ and stochastic diffusion losses $\propto (\tilde{B}_r/B_0)^2$ which was not apparent in the simple simulation scenario of Section IV.2.

Figure 8a shows the initial density $n_\alpha(r) \sim e^{-4\psi/\psi_{bd}}$ for an ensemble of 512 alphas with $\alpha = E_{\alpha o} = 3.5$ MeV. Taking $\tilde{\alpha} = 2 \times 10^{-3}$, the final density after 1000 $\tau_{transit}$ is shown in Fig. 8b. Note the substantial broadening of $n_\alpha(r)$ whose gradient drives the linear TAE instability growth rate.[9] As in the circular equilibrium case (cf. Fig. 7b) after 1000 $\tau_{transit}$ we observe that the TAE mode structure does not resonantly scatter alphas below $E_\alpha \simeq 1.5$ MeV thus dashing any hope for He-ash removal (desired for $E_\alpha \lesssim E_{crit} \sim 800$ keV). Figure 9 shows the pitch variable $\frac{v_\parallel}{v}$ of exiting alphas as they cross the loss boundary. One observes a peak at $\frac{v_\parallel}{v} \simeq 0.6$ which corresponds to a barely trapped α on the way to the wall. Inspecting Fig. 5b it becomes apparent that this α particle had $\frac{v_\parallel}{v} = -0.6$ before it went through its banana tip. And values of $\frac{v_\parallel}{v} \simeq -0.6$ correspond to barely passing alphas in resonance with the TAE on the outboard side of its orbit. This confirms our

previous observation of the predominance of this resonant orbit transformation for the overall losses driven by the TAE. Independently, Zweben et al[28] have isolated this orbit transformation as important in TFTR experiments on energetic single ion losses. Figure 10 shows the total number of lost alphas vs. time, clearly showing a steady state loss rate of $\simeq 4$ particles per unit time out of 512. (We have cross-checked this rate with runs with ≥ 1024 alphas.) Figure 10 (running for 5000 $\tau_{transit}$) supercedes the result of Fig. 7c and we stress again that in Fig. 10 lost alphas are **not** replaced by new randomly born alphas and prompt first orbit losses are not admitted. The initial transient in Fig. 10 is due to the resonant drift losses of alphas born near the loss boundary which was the dominant loss mechanism for the first simulation of Section IV.2. The subsequent steady state loss rate is due to fluctuation driven diffusion to the loss boundary.

For a deeper understanding, we return to Fig. 2 showing the α loss boundaries in $P_\varphi - \lambda$ space which was the topic of Part I (Ref. 22) of the present work. Figure 11b of Ref. 22 contains the (P_φ, λ) values of **exiting** alphas (dots). The analytically predicted loss boundary is shown in Fig. 5 of Ref. 22. (The excellent agreement between the analytic and the simulation boundary also serves to confirm the accuracy of the ORBIT code used here.) Figure 11a of Ref. 22 shows the **initial** (P_φ, λ) values of the later exiting alphas. Those initially far removed from the loss boundary have stochastically diffused to the boundary, rather than making it across by resonant drift. This diffusion is demonstrated and analyzed in detail in Part I of Ref. 22.

To determine the TAE amplitude threshold for the onset of stochastic diffusion, the mean square phase space displacements $\langle(\Delta P_\varphi)^2\rangle$ and $\langle(\Delta E)^2\rangle$ were measured as a function of time. Figure 12a of Ref. 22 shows $\langle(\Delta P_\varphi)^2\rangle$ for $\tilde{\alpha} = 2\times 10^{-4}$ where it is practically zero (note the scale factor 10^{-7}) and Fig. 12b of Ref. 22 for $\tilde{\alpha} = 2\times 10^{-3}$ where it becomes linear in time after the first 200 transit times. A similar behavior is observed for $\langle(\Delta E)^2\rangle$ vs. t, for $\tilde{\alpha} = 2\times 10^{-4}$ to 2×10^{-3}. This places the stochastic threshold at about $\tilde{\alpha}_{crit} \simeq 10^{-3}$, in accord with an **analytic** map criterion given in Ref. 21. Numerically, the onset of stochasticity is demonstrated in the stochastic maps shown in Figs. 14 in Ref. 22. An elementary derivation (contained in Ref. 22) proves $D_{P\varphi P\varphi} \equiv \langle(\Delta P_\varphi)^2\rangle/2t \propto (\tilde{B}_r/B_0)^2 q_{gap}^2$

and indeed, the Monte Carlo simulation of 512 alphas exhibits that the diffusion coefficient scales as $(\tilde{B}_r/B_0)^2$, as shown in Fig. 13 of Part I (Ref. 22). Concomitantly , the number of lost alphas, N_α (lost), also scales as B_r^2, see Fig. 11. A second run over 5000 $\tau_{transit}$ proves the expected linear increase of N_α with run time. This value of $N_\alpha^{lost}(t)$ corresponds to a loss frequency $\nu_L = \frac{1}{N_\alpha}\frac{dN_\alpha}{dt} = \frac{\Delta N_\alpha}{N_\alpha \Delta t} = 14/\text{sec}$ (taking $\Delta t = 1000\tau_{transit}$ where $\tau_{transit} \equiv \frac{2\pi R_0}{v_\alpha} = 0.8 \times 10^{-6}$) for $\frac{\tilde{B}_r}{B_0} = 1 \times 10^{-3}$. With the α slowing down time $\tau_{SD} = 0.180$ sec this yields $\nu_L \tau_{SD} = 0.25$ an estimated average radial diffusion coefficient $D_\alpha = a^2\nu_L/4 \simeq 1.1$ m^2/sec. Also, using Fig. 13 of Ref. 22, D_α can be roughly estimated from D_{pp} through renormalization by the factor $\frac{a^2}{(\psi_{pb})^2 \tau_{transit}}$. At $\frac{\tilde{B}_r}{B} \simeq 1 \times 10^{-3}, D_\alpha \simeq 1.6$ m^2/sec, which agrees with the estimation from N_α^{lost}.

V. SUMMARY AND CONCLUSIONS

A single toroidal mode number $n = 1$ toroidal Alfvén eigenmode (but containing all important poloidal mode numbers and their radial mode profiles calculated with the Nova-K code) is prescribed with certain mode amplitudes $10^{-4} \leq \tilde{B}_r/B_0 \leq 2 \times 10^{-3}$. A Hamiltonian guiding center code ORBIT (using a 4th order Runge Kutta algorithm tested as described Appendix B) is used to study (i) single α orbits and (ii) ensembles of up to 5000 particles following their orbits in the finite amplitude time dependent TAE fluctuations $(\tilde{A}_\parallel, \tilde{\varphi})$. Randomized (Monte Carlo) initial conditions are used to study phase space averaged behavior. Two CIT-like tokamak equilibria were used (cf. Appendix A for parameters). The main findings for the energetic fusion alphas are as follows:

(i) For alphas with $v_{\parallel\alpha} \sim v_A$ the parallel shear Alfvén resonance $\omega - k_\parallel v_{\parallel\alpha} - \mathbf{k}_\perp \cdot v_{D\alpha} = 0$ (where $\omega = v_A k_{\parallel gap}$ is the TAE (gap) frequency) leads to resonant energy exchange and resonant radial drift, proportional to $\tilde{B}_r/B_0$. If $\tilde{B}_r/B_0$ exceeds a threshold stochastic orbit diffusion occurs even for only one toroidal mode number. (See discussion in Ref. 22, i.e. Part I of this work.)

(ii) Toroidal angular momentum diffusion $D_{P_\varphi P_\varphi}$ and energy diffusion D_{EE} scales $\propto \tilde{B}_r^2$ and inversely with the square of the plasma current inside the gap radius.

(iii) Depending on (E, μ) and mode amplitude, the P_φ vs. φ action-angle plot shows stochastic regions clearly bounded by KAM surfaces. However, alphas in the stochastic domain can remain confined (although diffusing within a bounded region). This phase space location dependence of stochastic losses makes a uniform analytic description of $D_{P_\varphi P_\varphi}(E, \mu, P_\varphi)$ difficult.

(iv) An α particle whose unperturbed P_φ is close enough to a loss boundary can drift resonantly into the loss region if the corresponding KAM surface touches the loss boundary at a $\tilde{B}_r/B_0$ value even below the stochastic threshold. Such losses scale as $\tilde{B}_r$ (not $\tilde{B}_r^2$) and tend to vanish after a transient unless alphas are replenished by the fusion source or collisions. The stochastic threshold depends on (E, μ, P_φ) and the radial profile of the TAE which for low mode numbers typically peaks in the plasma core. Thus the core can be stochastic while the plasma edge still possesses KAM surfaces which cannot be crossed. Correspondingly, the total number of lost alphas N_α (lost) $\propto \left(\frac{\tilde{B}}{B_0}\right)$ in the initial transient phase of near boundary losses (lasting for $\approx 50\ \tau_{transient}$ and N_α (lost) $\propto \left(\frac{\tilde{B}}{B_0}\right)^2$ in the following steady state diffusion phase.

(v) The statistically most likely loss process is the fluctuation driven conversion of resonant counter-going circulating alphas near the passing/trapped boundary $\left(\frac{v_\parallel}{v} \simeq -0.6\right)$ to large trapped orbits. The conversion occurs because of the large resonant change of E_α (and thus the pitch angle parameter $r = \frac{\mu B_0}{E}$). The stochastic threshold depends on $\lambda = \frac{\mu B_0}{E}$, $\sigma = \frac{v_\parallel}{|v_\parallel|}$ e.g., for $\lambda = 0.8, \sigma = -1$, $\frac{\tilde{B}_r}{B_0}$ (threshold) $\geq 10^{-3}$ for the $n = 1$ TAE and fixed $E_{\alpha o} = 3.5$ MeV.

(vi) After 1000 $\tau_{transit}$ an initially peaked $n_\alpha(r)$ is broadened, depending on $\tilde{\alpha}$. (We vary $2 \times 10^{-4} \leq \tilde{\alpha} \equiv \frac{A_\parallel}{R_0 B_0} \leq 2 \times 10^{-3}$, or $10^{-3} \leq \frac{\tilde{B}_r}{B_0} \leq 10^{-2}$).

(vii) For a squared Gaussian $n_\alpha(r)$ initial profile, at $\tilde{\alpha} = 2 \times 10^{-3}$, the absolute loss fraction is $\frac{150}{512}$ in 5000 $\tau_{transit}$. (For CIT parameters this corresponds to 4 ms vs. $\tau_{SD} \simeq 180$ ms). Scaled back to $\tilde{\alpha} = 4 \times 10^{-4}$ which corresponds to a more typical $\frac{\tilde{B}_r}{B_0} = 2 \times 10^{-3}$ this yields a loss fraction of 52% in one slowing down time. For a broader trapezoidal $n_\alpha(r)$ the loss fraction is $\frac{255}{512}$ or 88%. This indicates the advantage of using peaked α

source profiles for good energetic α confinement.

(viii) No anomalous α transport below $\simeq$ 1.5 MeV is observed in the simulation which implies that resonant α TAE interaction is not useful for He-ash removal.

Acknowledgments

This work was supported by the US Department of Energy under Grant# DE-FG02-91ER-54109.

Appendix A
CIT Equilibrium Parameters

The ORBIT code following the Hamiltonian α guiding centers was run using two different (CIT-like) equilibria:

Equilibrium A is circular, with $a = 0.55$ m, $R_0 = 1.75$ m, $B = 10$ T, $q(0) = 1.01, q(a) = 3.4$ and a q-profile which is relatively flat out to 1/2 of the minor plasma radius. $n(0) = 5 \times 10^{20}$ m^{-3}, $T(0) = 15$ keV. (For this case, $\tau_{SD} = 40$ ms, $\langle \sigma_f v \rangle$ (at $\overline{T} = 10$ keV) $= 1.1 \times 10^{-16}$ cm^3/s. $\Omega_\alpha = 4.8 \times 10^8, \tau_{transit} \equiv \left(\frac{v_\alpha}{2\pi R_0}\right)^{-1} = .85 \times 10^{-6}$ s, $\omega_A = 1 \times 10^6, \tau_{fus} = \frac{1}{n_\alpha} \frac{\partial n_\alpha}{\partial t}\Big|_{fus} = 17$ ms $\lesssim \frac{1}{2}\tau_{SD}$.)

Equilibrium B is D-shaped with the same a, R_0, B and $q(\psi)$ profile. Elongation $\kappa = 2$, triangularity $\delta = 0.25$, with the same $n(0)$ and $T(0)$.

Appendix B

Numerical Accuracy of Orbit Integrator

The fourth order Runge Kutta algorithm was tested in several ways. Sensitive types of perturbed drift orbits such as stagnation orbits and pinch orbits (see Fig. 12) were followed over 30 $\tau_{transit}$ and remained stable to an accuracy of 10^{-5}. Energy conservation for zero fluctuation amplitude was within $\frac{\Delta E_\alpha}{E_{\alpha o}} = 3 \times 10^{-14}$ in 30 $\tau_{transit}$. The time t_0 for a single α to exit on a loss orbit was tested as a function of the internal orbit stepsize Δt. $t_0/\tau_{transit}$ remained constant within $\pm 15\%$ upon halving Δt from $\Delta t/\tau_{transit} = \frac{1}{20}$ to $\frac{1}{40}$. More saliently, the Poincaré plots retained excellent stability for $\Delta t/\tau_{transit}$ changing from $\frac{1}{10}$ to $\frac{1}{20}$. The phase space diffusion coefficient $D_{P_\varphi P_\varphi}$ and the total number of alphas lost, N_α^{lost}, were stable under the change $\Delta t/\tau_{transit} = \frac{1}{10}$ to $\frac{1}{40}$. Finally, N_α^{lost} after 5000 $\tau_{transit}$ proved equal to $5 \times N_\alpha^{lost}$ after 1000 $\tau_{transit}$ as it should.

References

[1]A. B. Mikhailovskii, Sov. Phys. JETP **41**, 890 (1975).

[2]M. N. Rosenbluth, P. H. Rutherford, Phys. Rev. Lett. **34**, 1428 (1975).

[3]K. T. Tsang, D. J. Sigmar, J. C. Whitson, Phys. Fluids **24**, 1508 (1981).

[4]K. L. Wong, R. J. Fonck, S. F. Paul, D. R. Roberts, E. D. Fredrickson, R. Nazikian, H. K. Park, M. Bell, N. L. Bretz, R. Budny, S. Cohen, G. W. Hammett, F. C. Jobes, D. M. Meade, S. S. Medley, D. Mueller, Y. Nagayama, D. K. Owens, E. J. Synakowski, Phys. Rev. Lett. **66**, 1874 (1991).

[5]W. W. Heidbrink, E. J. Strait, E. Doyle, G. Sager, R. T. Snider, Nucl. Fus. **31**, 1635 (1991).

[6]C. E. Kieras, J. A. Tataronis, J. Plasma Phys. **28**, 395 (1982).

[7]C. Z. Cheng, L. Chen, M. S. Chance, Ann. Phys. (NY) **161**, 21 (1985).

[8]C. Z. Cheng, M. S. Chance, Phys. Fluids **29**, 3695 (1985).

[9]G. Y. Fu, J. Van Dam, Phys. Fluids **B1**, 1949 (1989).

[10]D. J. Sigmar, C. T. Hsu, R. White, C. Z. Cheng, (Proceedings of Technical Committee Meeting in Kiev, October 1989, International Atomic Energy Agency, Vienna) Vol. II, p. 457.

[11]R. R. Parker, G. Bateman, P. L. Colestock, H. P. Furth, R. J. Goldston, W. A. Houlberg, D. Ignat, S. Jardin, J. L. Johnson, S. Kaye, C. Kieras-Phillips, J. Manickam, D. B. Montgomery, R. Myer, M. Phillips, R. Pillsbury, N. Pomphrey, M. Porkolab, D. E. Post, P. H. Rutherford, R. Sayer, J. Schmidt, G. Sheffield, D. J. Sigmar, D. Stotler, D. Strickler, R. Thome, R. Weiner, J. C. Wesley, Plas. Phys. Contr. Nucl. Fus. Res. **3**, 341, IAEA, Vienna, 1989.

[12]K. Tomabechi, Plas. Phys. Contr. Nucl. Fus. Res. **3**, 214, IAEA, Vienna, 1989.

[13]C. Z. Cheng, Phys. Fluids **B2**, 1427 (1990) and Phys. Fluids **B3**, 2463 (1991).

[14]R. Betti, J. P. Freidberg, Phys. Fluids **B3**, 538 (1991); **B3**, 1865 (1991), third paper on kinetic theory of linear growth rate of toroidal Alfvén eigenmodes submitted to Phys. Fluids (1991).

[15]H. L. Berk, B. N. Breizman, Phys. Fluids **B2**, 2246 (1990).

[16]H. L. Berk, B. N. Breizman, H. Ye, submitted to Phys. Rev. Lett. (1991).

[17]A. I. Morozov, L. S. Solovév in Reviews of Plasma Physics, (Consultants Bureau, New York, 1966) Vol. 2, p. 201.

[18]R. G. Littlejohn, Phys. Fluids **28**, 2015 (1985).

[19]R. B. White, A. H. Boozer, R. Hay, Phys. Fluids **25** 575 (1982).

[20]R. B. White, in "Theory of Tokamak Plasmas," North Holland, New York, 1989.

[21]B. N. Breizman, H. L. Berk, H. Ye, private communication, 1991.

[22]C. T. Hsu, D. J. Sigmar, submitted to Phys. Fluids B as Part I of the present work (1991).

[23]K. W. Gentle, Fusion Technology **1**, 479 (1981).

[24]D. J. Grove, D. M. Meade, Nucl. Fusion **25**, 1167 (1985).

[25]K. Bol, M. Okabayashi, R. Fonck, Nucl. Fusion **25**, 1149 (1985).

[26]M. F. F. Nave, D. J. Campbell, E. Joffrin, F. B. Marcus, G. Sadler, P. Smeulders, K. Thomsen, Nucl. Fusion **4**, 697 (1991).

[27]F. Y. Gang, D. J. Sigmar, J. N. Leboeuf, Phys. Letters (1991), accepted for publication, February 1992.

[28]S. J. Zweben, R. Boivin, C. S. Chang, G. Hammett, H. E. Mynick, cf. Fig. 1 in Nucl. Fusion **31** (1992), accepted for publication.

Table 1

α Loss Rate ν_L for $\tilde{\alpha} \equiv \frac{1}{5}\frac{\tilde{B}_r}{B_o}$

E_o ↓ $\tilde{\alpha}$ →	10^{-3}	5×10^{-4}	10^{-4}
$3.52 \rightarrow 2.52$	3×10^3	1.2×10^3	250
$2.52 \rightarrow 1.52$	10^3	500	100
$1.52 \rightarrow 0.52$	40		

Figure Captions

Fig. 1: Examples of α orbits with $E_\alpha = 3.5$ MeV but various pitch values $v_\parallel/v$ in CIT equilibrium B (described in Appendix A). Note that the alphas near the trapped/passing separatrix have large orbit width even in this high magnetic field ($B = 10$ T) high current machine.

Fig. 2: Phase space topology of 3.5 MeV α particle in $P_\varphi - \lambda$ space. ($\lambda \equiv \mu B_0/E$). For example, an α crossing the heavy line which starts at $P_\varphi = -1.26$ (where P_φ is normalized to $\frac{e}{c}\psi_{boundary}$) is converted from a counter-going passing particle orbit to a trapped orbit which soon intersects the wall $\psi_p = \psi_{boundary}$.

Fig. 3: Radial eigenfunction of perturbed vector potential $\tilde{A}_\parallel$ for toroidal mode number $n = 1$, with relevant poloidal mode numbers $m = 1, 2, 3$ for circular plasma equilibrium described in Appendix A.

Fig. 4: Same for D-shaped equilibrium described in Appendix A.

Figures 5a,b,c show a resonant α in the circular equilibrium of Appendix A.

Fig. 5a: Resonant energy loss of fusion born α, due to TAE vs. time. $\tau_{transit} = 2\pi R_0/v_{o\alpha}$.

Fig. 5b: Resonant pitch change vs. time of same α. Note the conversion from a passing to a trapped orbit.

Fig. 5c: Orbit of the same α in $r - \theta$ space. Note the conversion and loss to the wall.

Figures 6a,b,c show a resonant α in the D-shaped equilibrium of Appendix A, analogous to Fig. 5.

Fig. 6a: The orbit in $\psi_p - \theta$ space.

Fig. 6b: Resonant energy change of the orbit.

Fig. 6c: Resonant pitch change.

Figures 7a,b,c: Monte Carlo simulation in circular equilibrium.

Fig. 7a: Monte Carlo simulation of 5120 alphas originally at $E_{\alpha o} = 3.5$ MeV, $\psi_T \equiv (r/a)^2/2 = 0.12$ (for the circular equilibrium), random pitch $\frac{v_\parallel}{v}$ and random poloidal angle. The TAE structure is shown in Fig. 2. $\tilde{B}_r/B_0 = 5 \times 10^{-4}$. After 200 $\tau_{transit}$ the α density $n_\alpha(r)$ is spread out as shown in the histogram.

Fig. 7b: TAE driven energy spread for the same case. Note that after 200 $\tau_{transit}$ (i.e. after $\approx$ 200 Alfvén wave periods since $\omega_A \approx \omega_{transit}$) there are still no alphas below $E_\alpha = 2.9$ MeV.

Fig. 7c: Number of alphas lost to the wall, vs. time. The first short transient is due to prompt orbit losses to the wall. The evolution thereafter mainly describes alphas born near the wall drifting resonantly across the prompt loss boundary. Each lost α is replaced by a new α randomly initialized in $\psi_p, \theta, \xi, v_\parallel/v$.

Figures 8a,b: Alpha particle density profiles.

Fig. 8a,b: Initial (Fig. 8a) and final (Fig. 8b) $n_\alpha(\psi_p)$ profile for the Monte Carlo simulation of 512 alphas using the D-shaped equilibrium B of Appendix A, running for 1000 $\tau_{transit}$. Note the substantial α profile broadening due to the TAE. $\tilde{\alpha} = 2 \times 10^{-3}$. The initial profile was $n_\alpha \propto \exp[-4\psi/\psi_{pb}]$, following n^2T^2.

Fig. 9: Number of exiting alphas vs. pitch $v_\parallel/v$. Again, note the predominance of nearly trapped (barely passing) alphas which are resonantly scattered into fat trapped alphas on loss orbits.

Fig. 10: Number of lost alphas N_α (lost) vs. time for a much longer running simulation (5000 $\tau_{transit}$) than that of Fig. 7c which spanned only the first 200 $\tau_{transit}$ during which resonant radial drift losses predominated. Over the longer time shown here, resonant diffusion losses in $P_\varphi - \lambda$ space transport alphas from all over phase space to the loss boundaries.

Fig. 11: Scaling of N_α (lost) with perturbed TAE amplitude $\delta B = \tilde{B}_r$. The constant $C = 2 \times 10^{-3}$. The observed scaling with $(\delta B)^2$ indicates the diffusive nature of the loss mechanism.

Fig. 12: Testing the accuracy of the orbit integrator on the delicate pinch orbit, over

30 $\tau_{transit}$. The pinch point remains stable. Similar stability is observed for stagnation orbits (see also Part I of this work.)

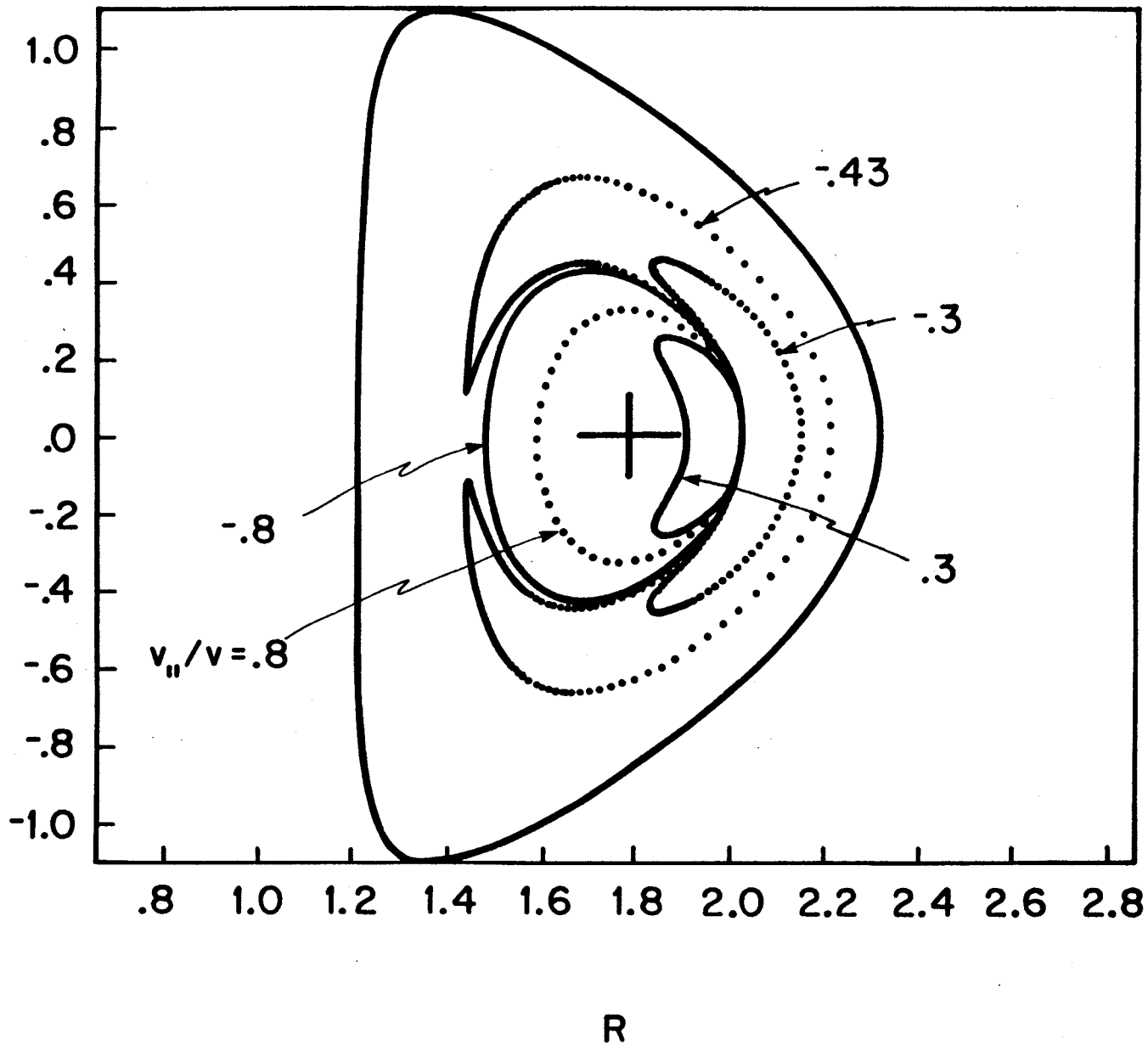
1.0
.8
.6
.4
.2
.0
-.2
-.4
-.6
-.8
-1.0
Z
.8
1.0
1.2
1.4
1.6
1.8
2.0
2.2
2.4
2.6
2.8
R
-.43
-.3
-.8
.3
$v_{\parallel}/v = .8$

Figure 1

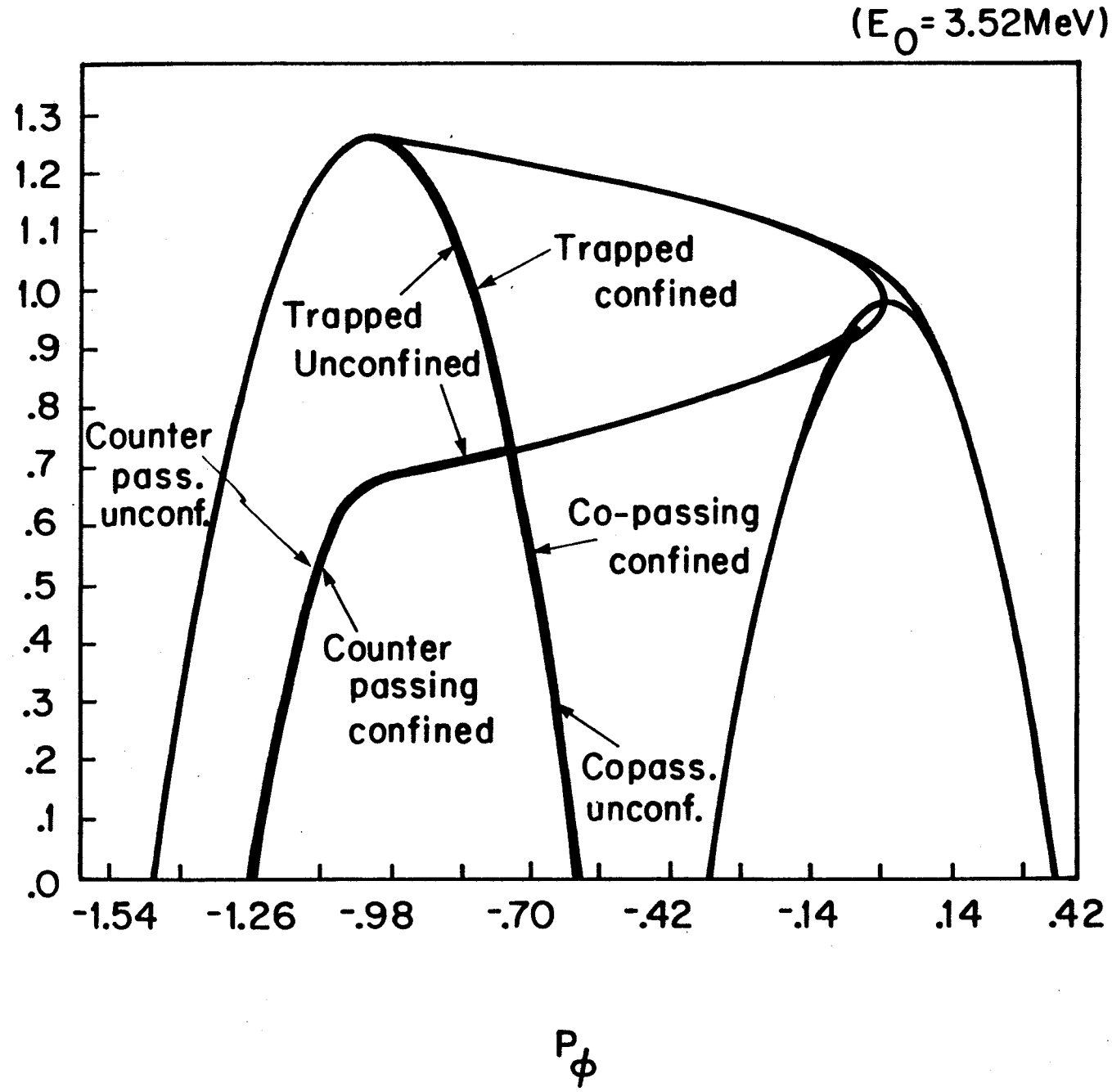
(E_0= 3.52MeV)
1.3
1.2
1.1
1.0
.9
.8
.7
.6
.5
.4
.3
.2
.1
.0
γ
Trapped
confined
Trapped
Unconfined
Counter
pass.
unconf.
Co-passing
confined
Counter
passing
confined
Copass.
unconf.
-1.54
-1.26
-.98
-.70
-.42
-.14
.14
.42
P_ϕ

Figure 2

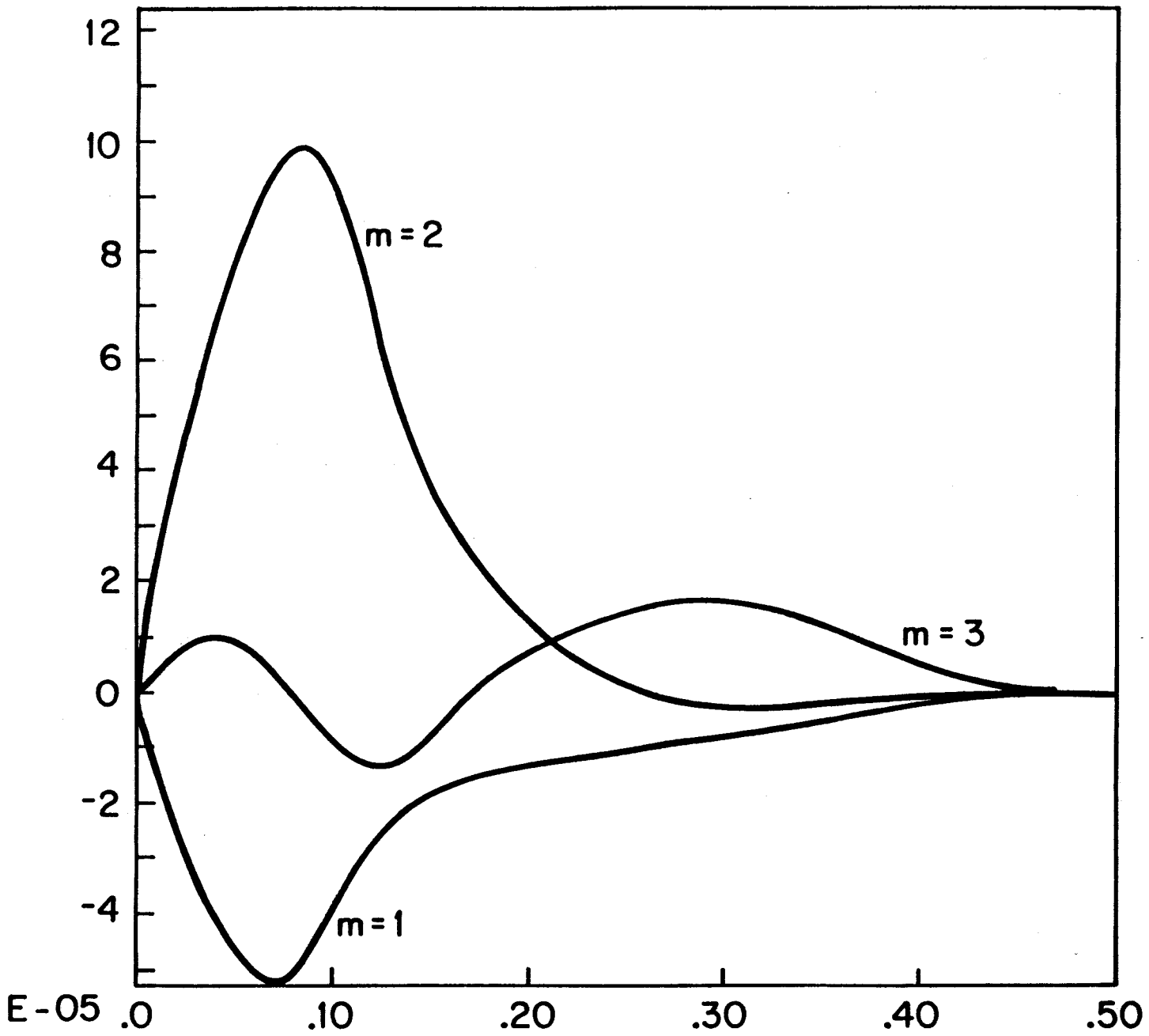

Figure 3

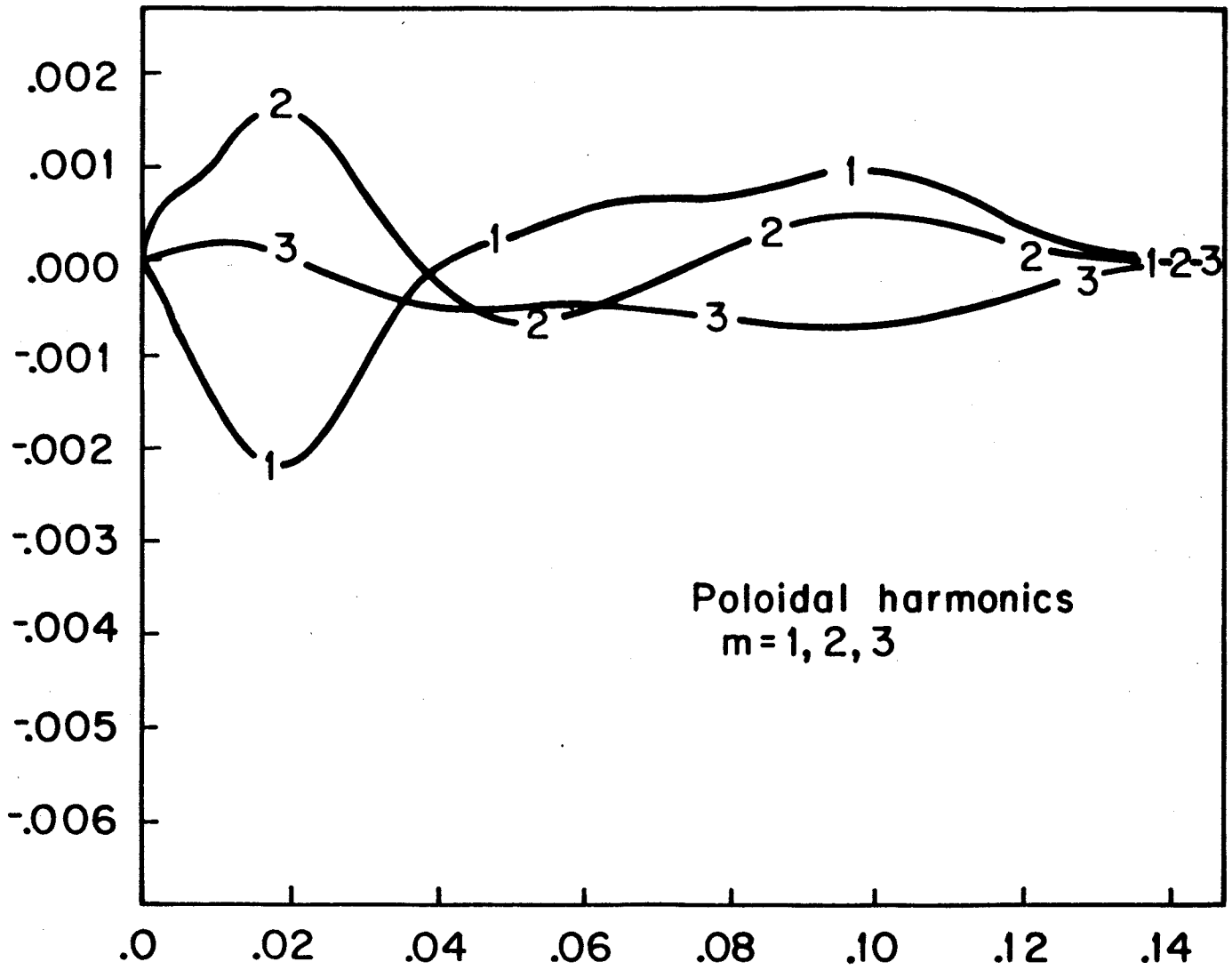
.002
.001
.000
-.001
-.002
-.003
-.004
-.005
-.006
.0
.02
.04
.06
.08
.10
.12
.14
Poloidal harmonics
m=1, 2, 3
1-2-3
ψ_p

Figure 4

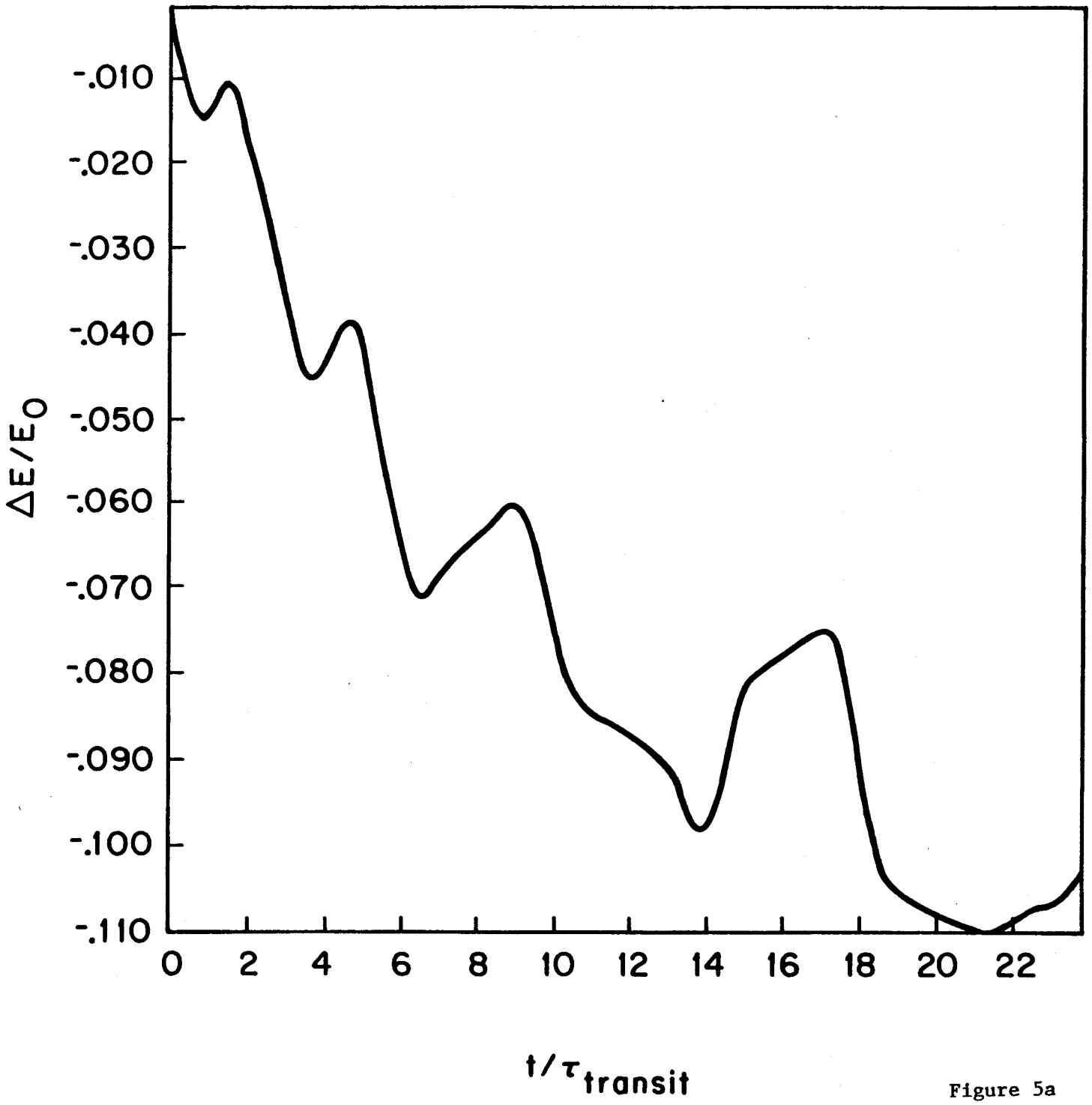
-.010
-.020
-.030
-.040
-.050
-.060
-.070
-.080
-.090
-.100
-.110
ΔE/E0
0
2
4
6
8
10
12
14
16
18
20
22
t/τtransit

Figure 5a

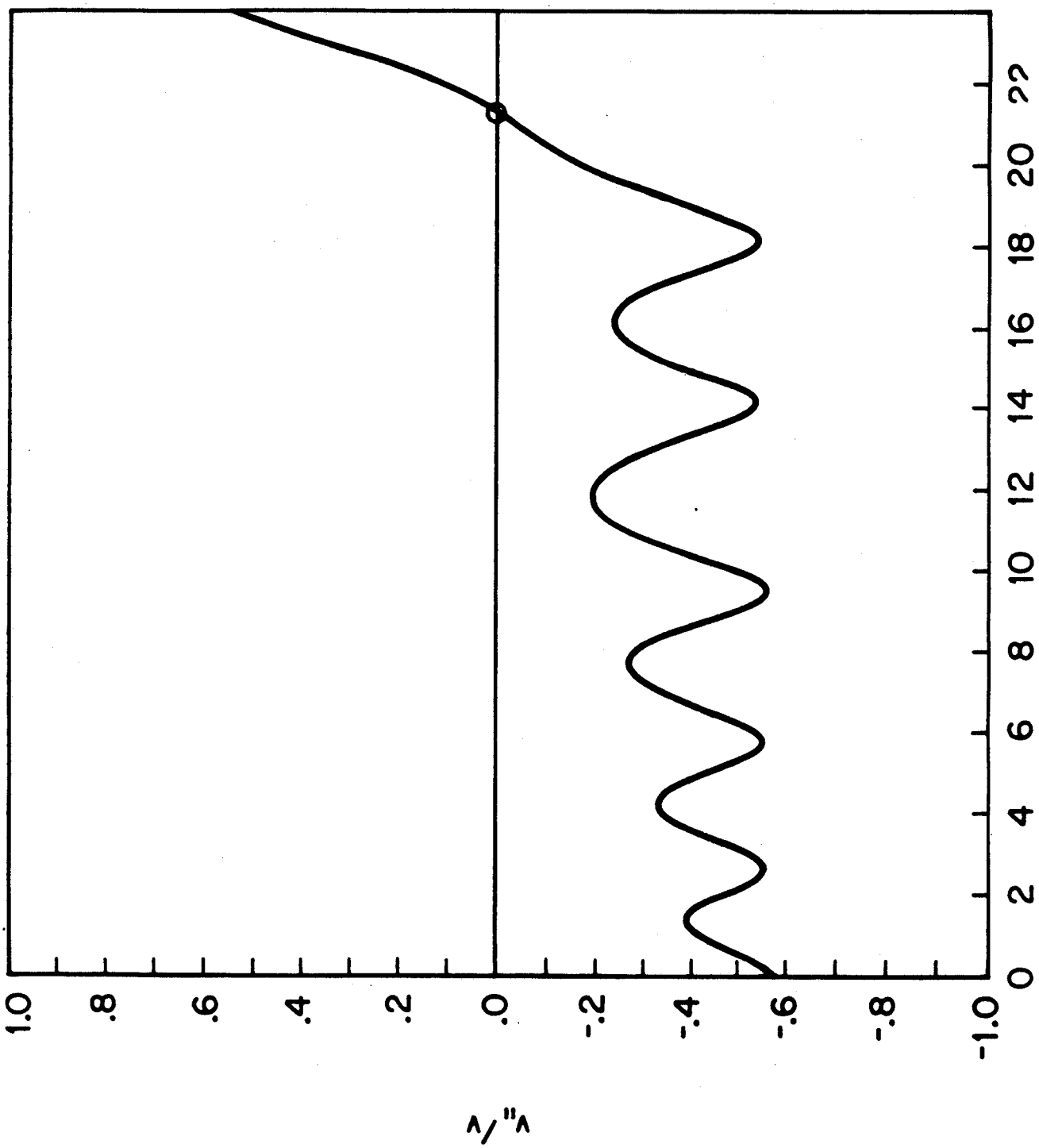

Figure 5b

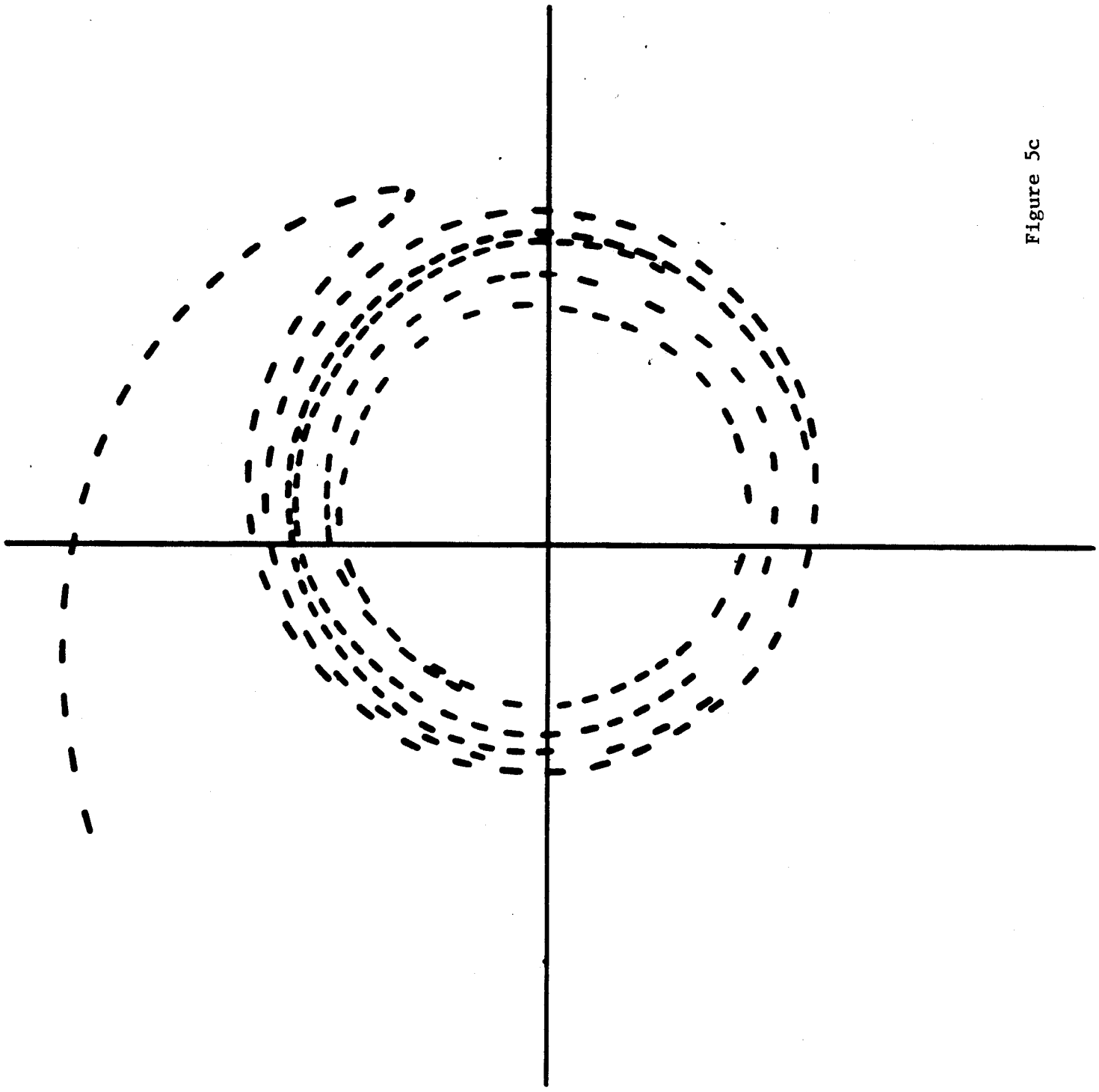

Figure 5c

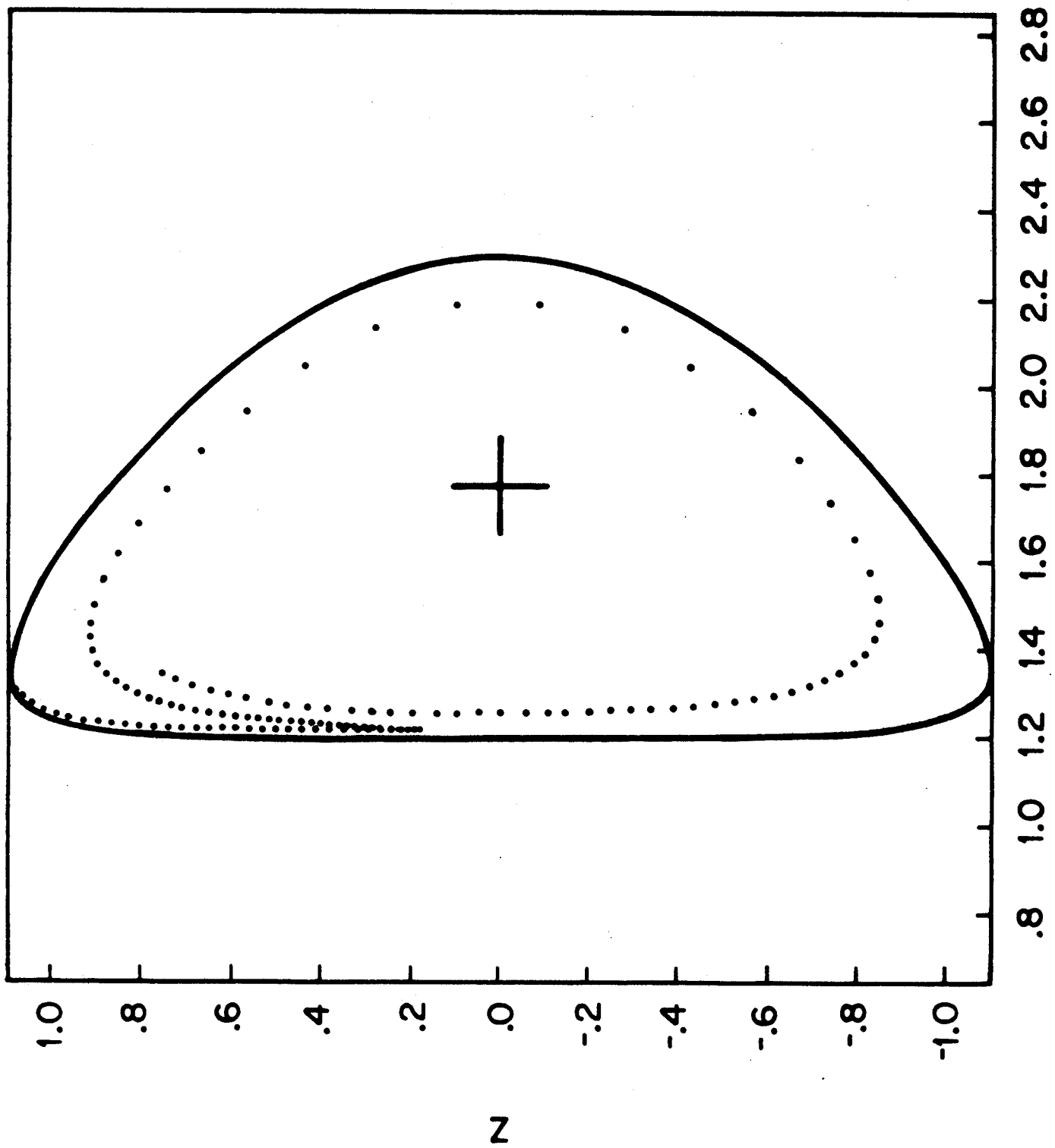

Figure 6a

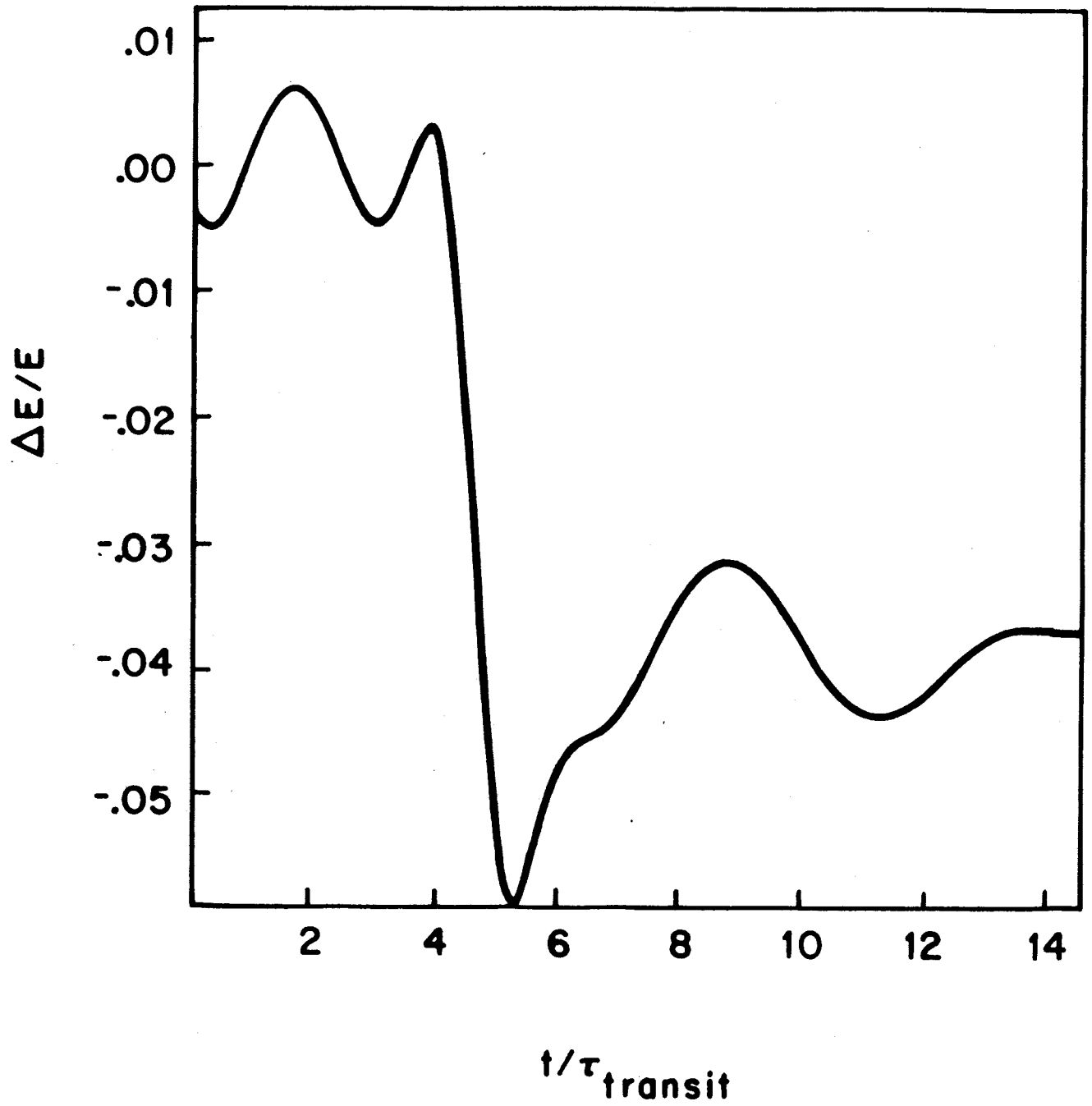

Figure 6b

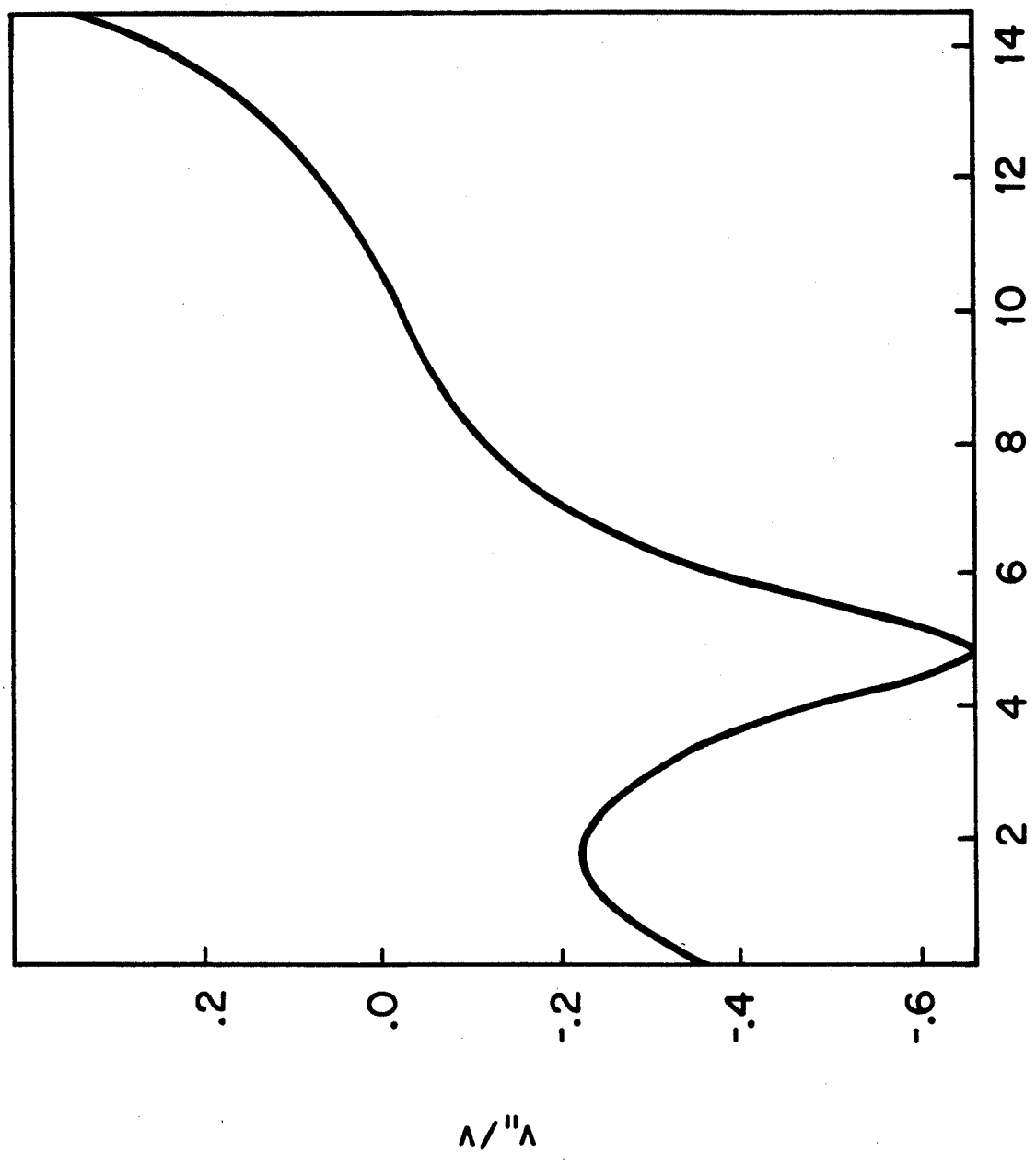

Figure 6c

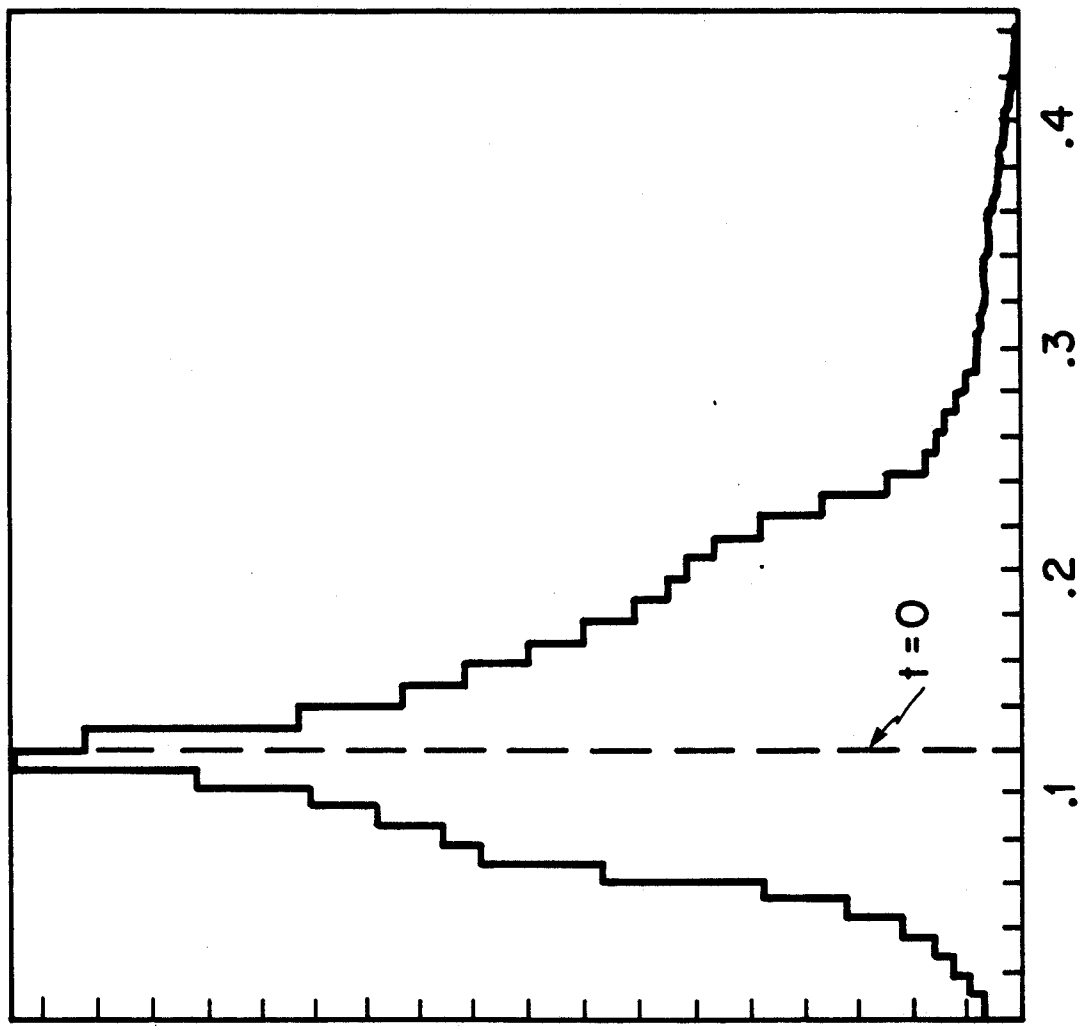

Figure 7a

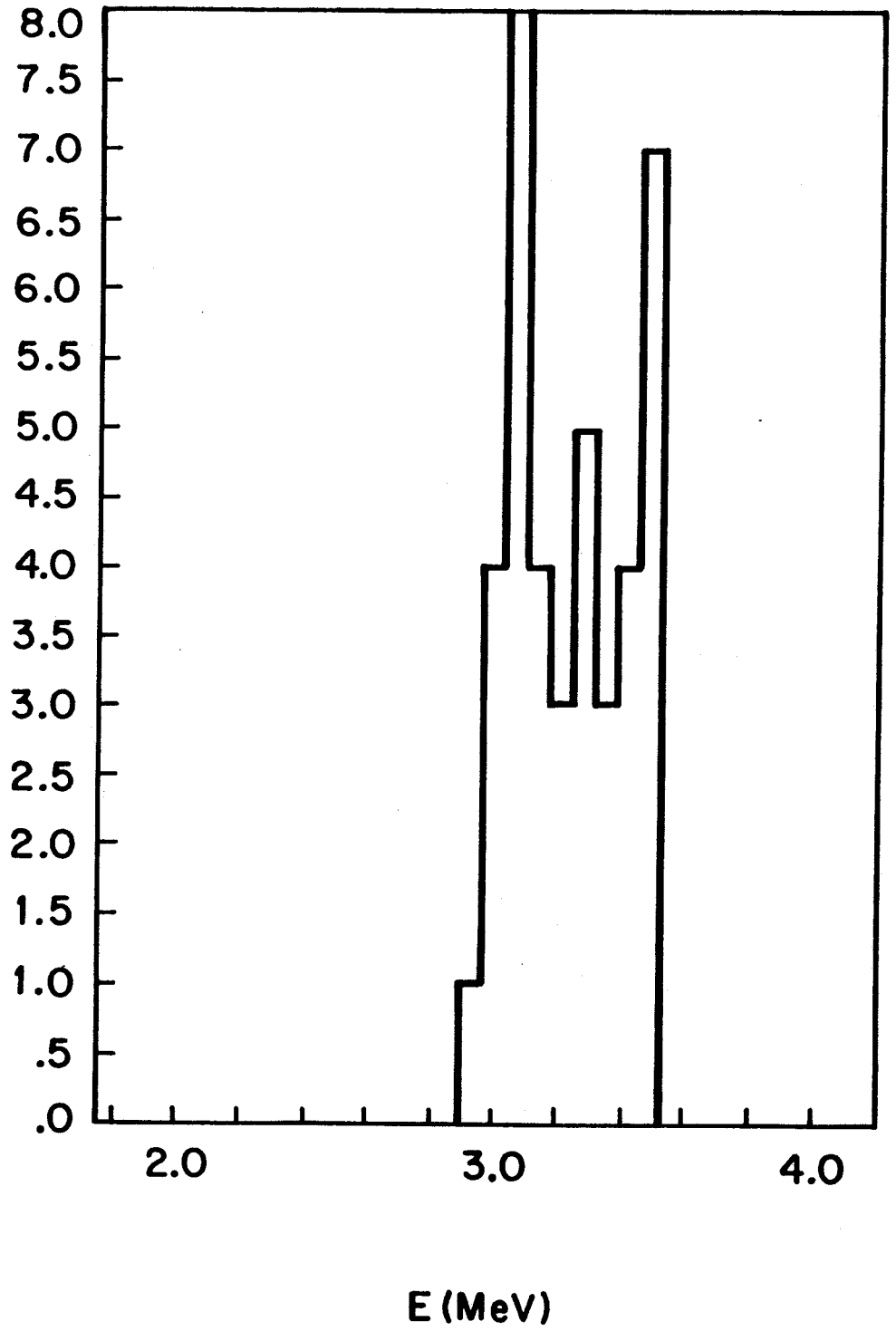

Figure 7b

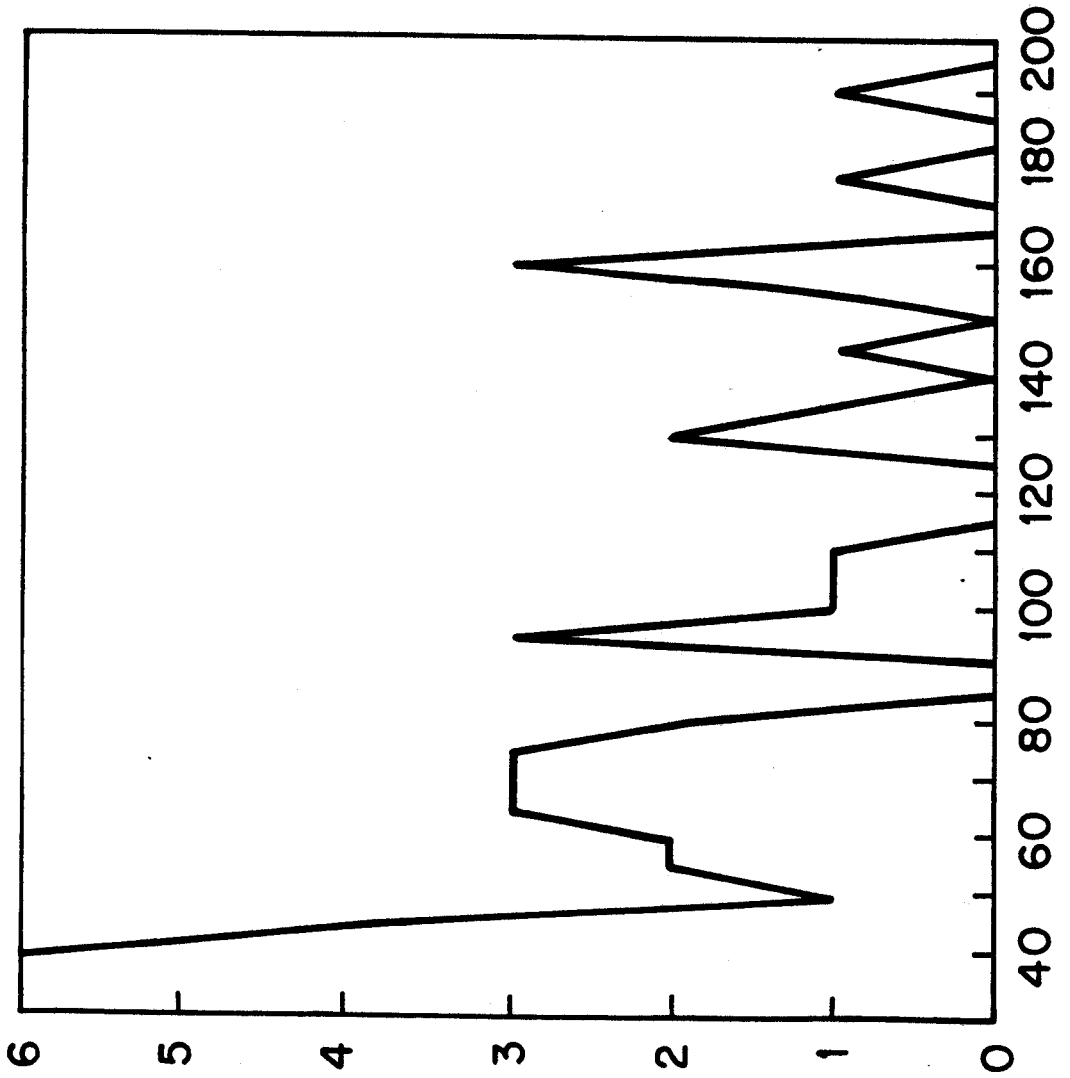

Figure 7c

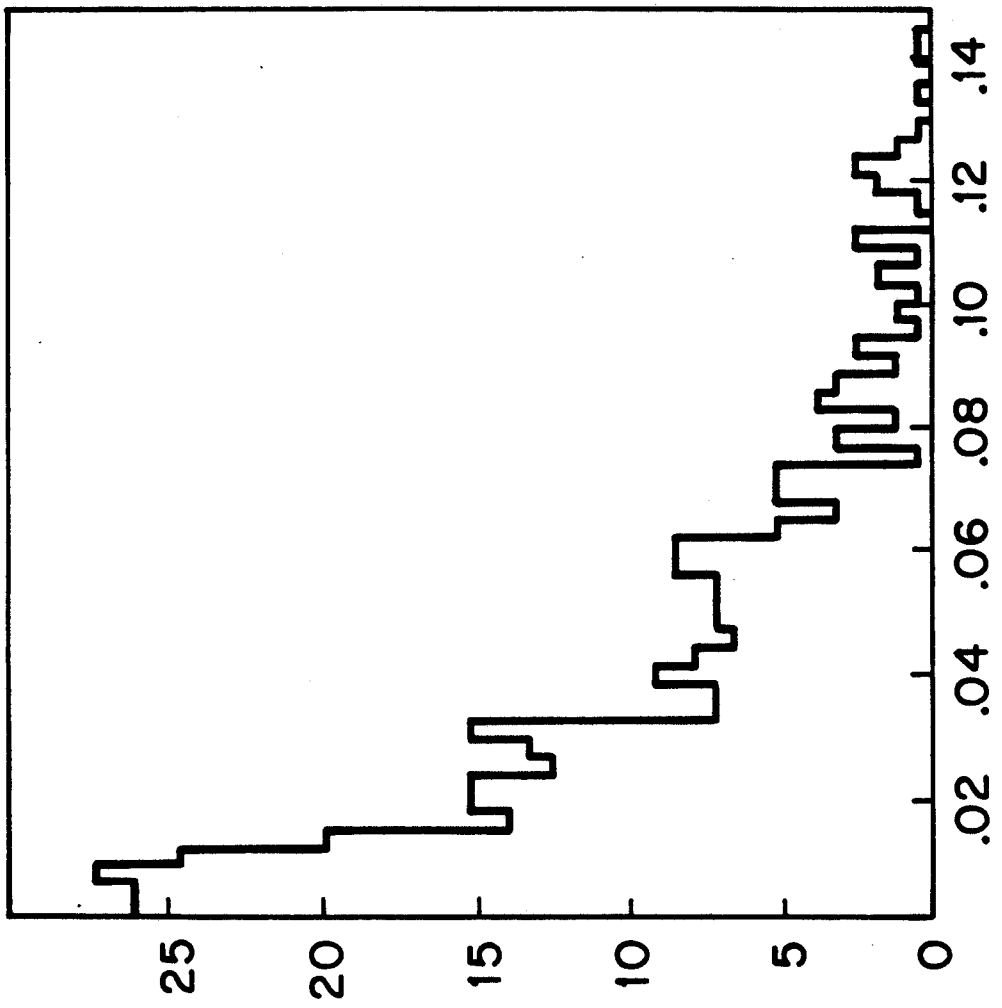

Figure 8a

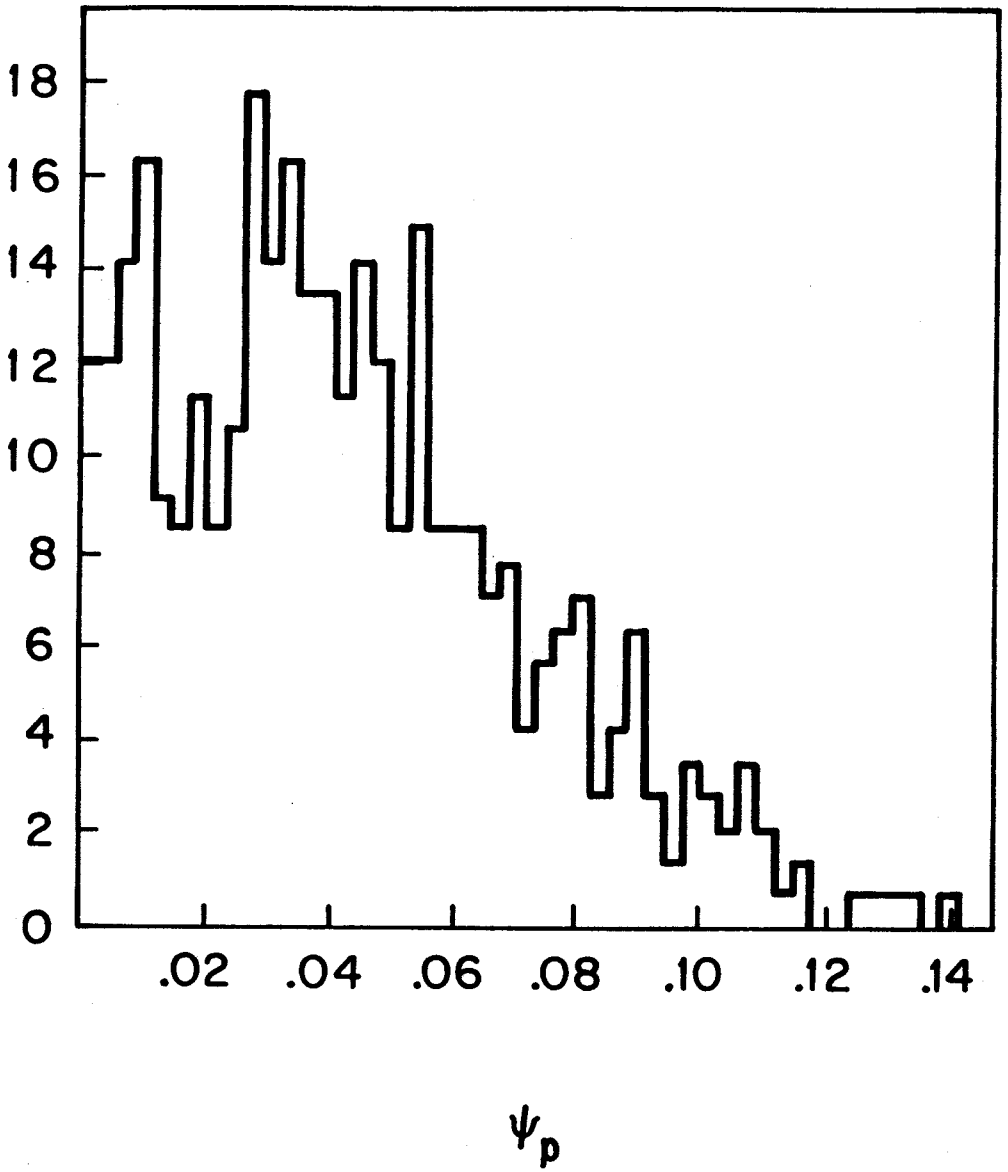

Figure 8b

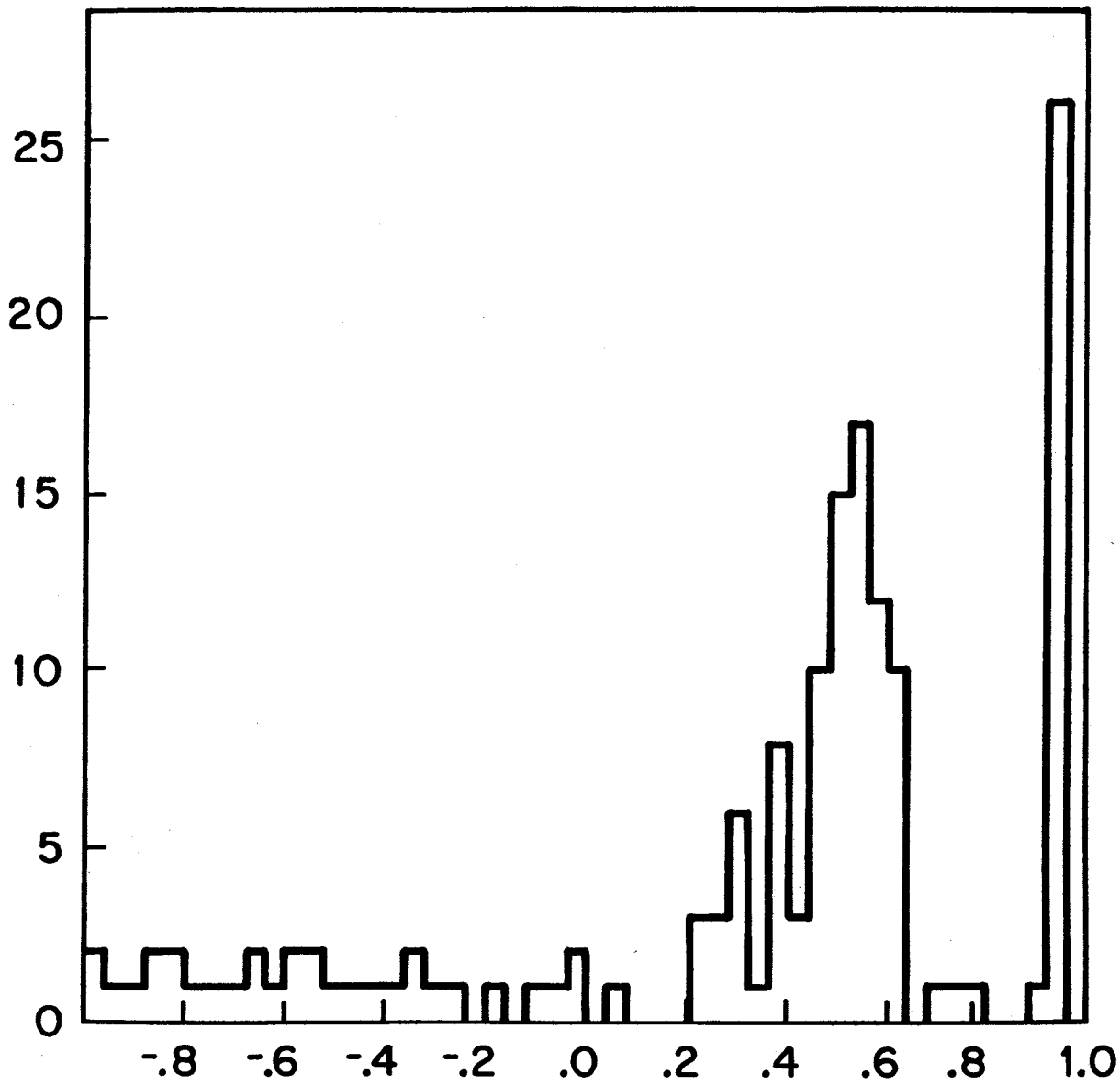

Figure 9

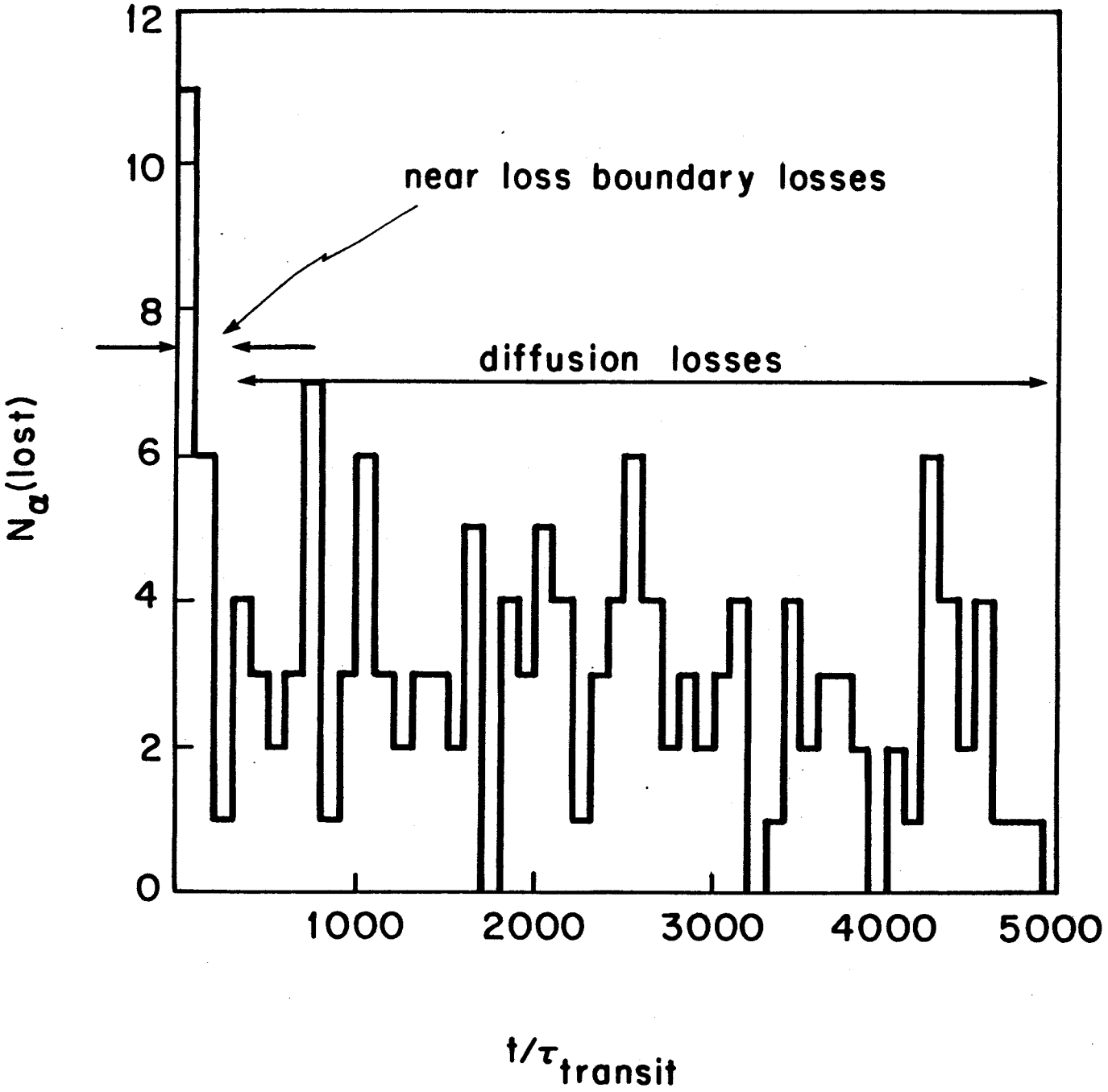
12
10
8
6
4
2
0
near loss boundary losses
diffusion losses
N_α(lost)
1000
2000
3000
4000
5000
$t/\tau_{transit}$

Figure 10

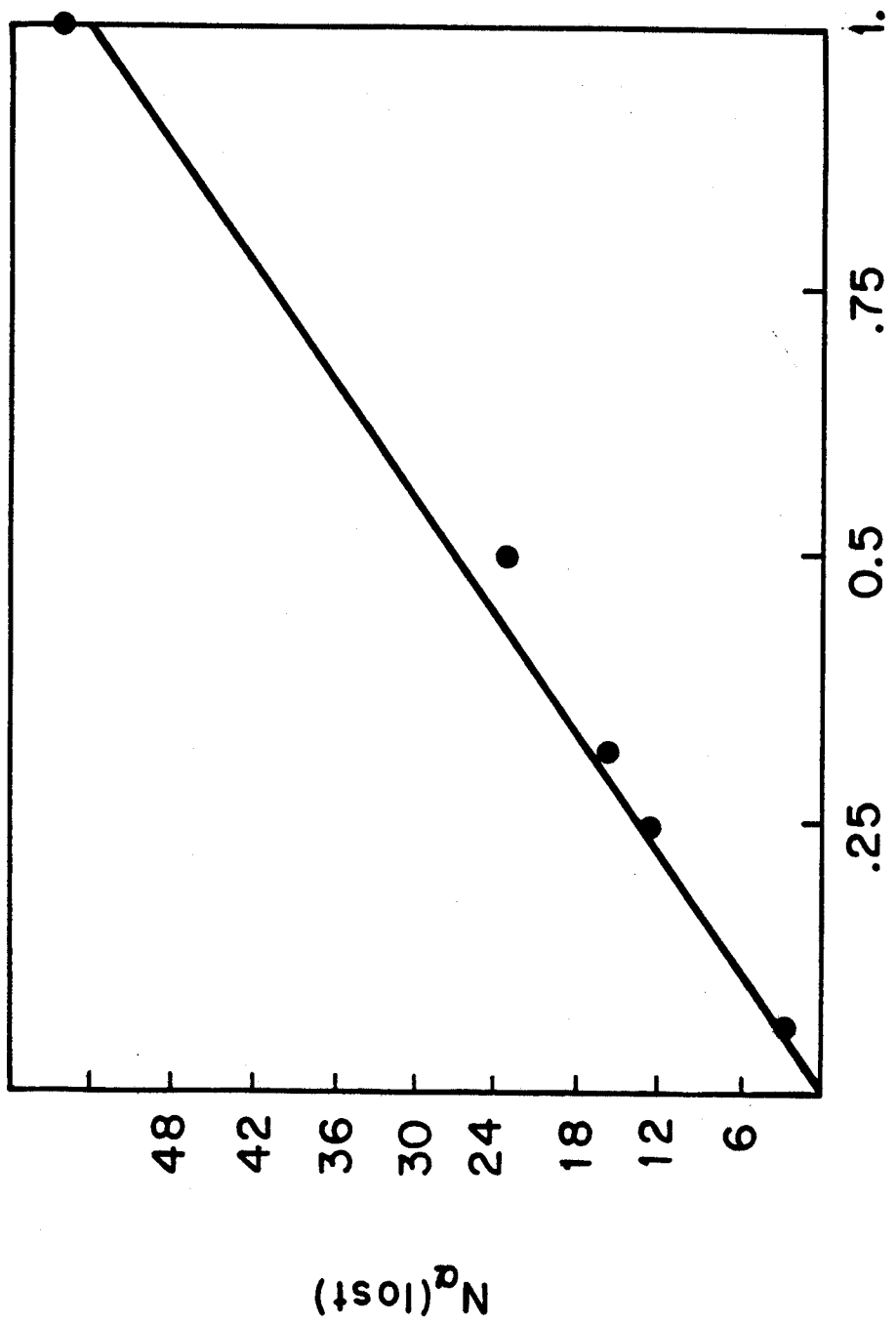

Figure 11

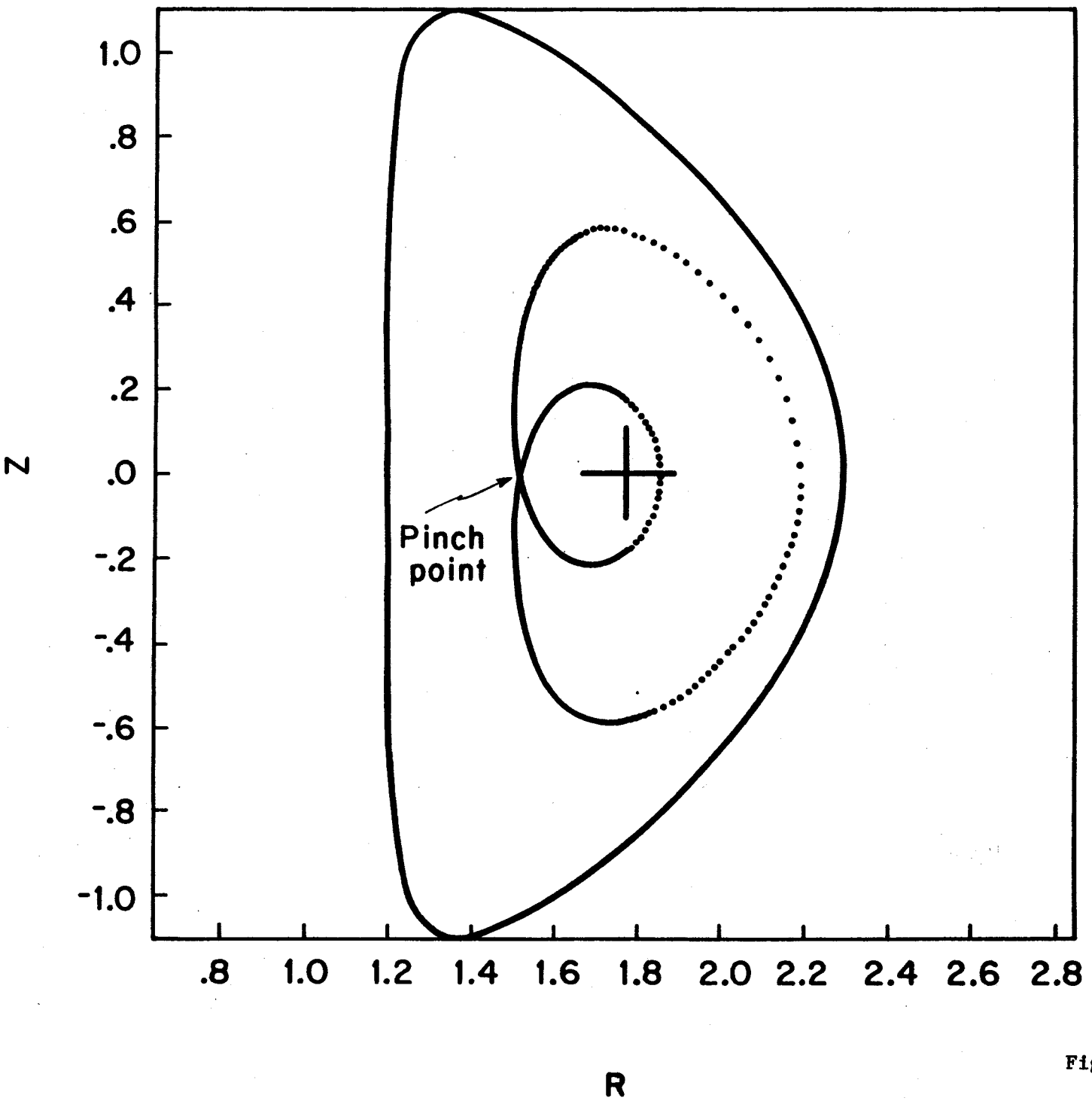

Figure 12